1-1-2014

Systems Modeling of Calcium Homeostasis and Mobilization in Platelets Mediated by Ip3 and Store-Operated Calcium Entry

Andrew Thomas Dolan
University of Pennsylvania, adolan@seas.upenn.edu

Systems Modeling of Calcium Homeostasis and Mobilization in Platelets Mediated by Ip3 and Store-Operated Calcium Entry

Abstract
Platelet aggregation is one of the body's first responses to vascular damage to prevent blood loss; upon injury to the endothelium platelets react to the exposed extracellular matrix and undergo a host of intracellular biochemical changes enabling them to activate and form a "plug" at the site of injury. Internally, platelets respond to their environment by exhibiting a sharp rise in cytosolic calcium that triggers a series of chemical and morphological changes which are critical to platelet activation and subsequent clot propagation. This thesis develops a mechanistic, computational model of platelet calcium regulation using coupled sets of ordinary differential equations. This thesis extends previous work modeling calcium release mediated by inositol 1,4,5-trisphosphate (IP_3) to engineer what is the first, to date, complete model of store-operated calcium entry (SOCE) integrated into a systems model for calcium signaling. SOCE is a ubiquitous extracellular calcium entry pathway which is activated by calcium store depletion, is seen in many cells types and is yet to be fully understood. Our model for SOCE regulation consists of diffusion-limited dimerization of the calcium sensor STIM1, followed by fast, cytosolic calcium-dependent association of STIM1 dimers with Orai1 channels in the plasma membrane resulting in graded store-operated channel activation. Appropriate model resting states were characterized using a dense Monte Carlo technique on an initial condition sampling space constrained by available data on species concentrations and protein copy numbers. From this set of resting configurations, following application of physiologic IP_3 stimuli, we selected for resting states exhibiting calcium dynamics that are in agreement with experimental data. We also selected for states presenting significant SOCE current based on differences in cytosolic calcium between simulations run with and without extracellular calcium. Low resting levels of IP_3 are required for system robustness and for simultaneous appropriate dynamic response to physiologic agonists. Platelets require a resting electrical potential across the membrane surrounding the calcium stores of greater than -70 mV in order to exhibit significant agonist-induced calcium release.

Degree Type
Dissertation

Degree Name
Doctor of Philosophy (PhD)

Graduate Group
Chemical and Biomolecular Engineering

First Advisor
Scott L. Diamond

Keywords
platelets, signal transduction, store-operated calcium entry, systems biology

SYSTEMS MODELING OF CALCIUM HOMEOSTASIS AND MOBILIZATION IN PLATELETS MEDIATED BY IP_3 AND STORE-OPERATED CALCIUM ENTRY

Andrew Thomas Dolan

A DISSERTATION

in

Chemical and Biomolecular Engineering

Presented to the Faculties of the University of Pennsylvania

in

Partial Fulfillment of the Requirements for the

Degree of Doctor of Philosophy

2014

Supervisor of Dissertation

_____

Scott L. Diamond

Professor, Chemical and Biomolecular Engineering

Graduate Group Chairperson

_____

Raymond J. Gorte, Professor, Chemical and Biomolecular Engineering

Dissertation Committee

Lawrence F. Brass, Professor, Department of Medicine

Matthew J. Lazzara, Assistant Professor, Department of Chemical and Biomolecular Engineering

Ravi Radhakrishnan, Associate Professor, Department of Chemical and Biomolecular Engineering

SYSTEMS MODELING OF CALCIUM HOMEOSTASIS AND MOBILIZATION IN PLATELETS MEDIATED BY IP_3 AND STORE-OPERATED CALCIUM ENTRY

ACKNOWLEDGMENT

This work would not have been possible without the support of numerous colleagues, family members, and friends. First I would like to thank my advisor, Dr. Scott Diamond, whose guidance, advice and support during my time here have been indispensible to me. I would also like to thank the members of my committee, Dr. Skip Brass, Dr. Ravi Radhakrishnan and Dr. Matt Lazzara for taking the time to sit on my committee and for their insights and advice. Special thanks also go to all members of the Diamond lab, past and present, with whom I have worked, learned from and become friends with, especially Dr. Tom Colace, Dr. Jeremy Purvis, Dr. Matt Flamm, Dr. Manash Chatterjee, Dr. Roman Voronov, Dr. Dan Jaeger, Ryan Muthard, Mei Yan Lee, John Welsh and Richard Li. Also thanks go to Huiyan Jing, our lab manager and phlebotomist who keeps everything running smoothly.

One of the most valuable things Penn has given me has been the friends I have made and the experiences we have shared; you are always appreciated even if I do not always seem to show it. Finally I would like to thank my parents, Jane and David, for being a source of unconditional love, delicious home cooked meals, and for being there whenever I was feeling down. The life lessons and values you taught me starting from childhood will always stay with me; the work ethics and sense of responsibility which you imparted to me truly helped me through these last few years.

ABSTRACT

SYSTEMS MODELING OF CALCIUM HOMEOSTASIS AND MOBILIZATION IN PLATELETS MEDIATED BY IP_3 AND STORE-OPERATED CALCIUM ENTRY

Andrew T. Dolan

Scott L. Diamond

Platelet aggregation is one of the body's first responses to vascular damage to prevent blood loss; upon injury to the endothelium platelets react to the exposed extracellular matrix and undergo a host of intracellular biochemical changes enabling them to activate and form a "plug" at the site of injury. Internally, platelets respond to their environment by exhibiting a sharp rise in cytosolic calcium that triggers a series of chemical and morphological changes which are critical to platelet activation and subsequent clot propagation. This thesis develops a mechanistic, computational model of platelet calcium regulation using coupled sets of ordinary differential equations. This thesis extends previous work modeling calcium release mediated by inositol 1,4,5-trisphosphate (IP_3) to engineer what is the first, to date, complete model of store-operated calcium entry (SOCE) integrated into a systems model for calcium signaling. SOCE is a ubiquitous extracellular calcium entry pathway which is activated by calcium store depletion, is seen in many cells types and is yet to be fully understood. Our model for SOCE regulation consists of diffusion-limited dimerization of the calcium sensor STIM1, followed by fast, cytosolic calcium-dependent association of STIM1 dimers with Orai1 channels in the plasma membrane resulting in graded store-operated channel activation. Appropriate model resting states were characterized using a dense Monte Carlo technique on an initial condition sampling space constrained by available data on species concentrations and

protein copy numbers. From this set of resting configurations, following application of physiologic IP_3 stimuli, we selected for resting states exhibiting calcium dynamics that are in agreement with experimental data. We also selected for states presenting significant SOCE current based on differences in cytosolic calcium between simulations run with and without extracellular calcium. Low resting levels of IP_3 are required for system robustness and for simultaneous appropriate dynamic response to physiologic agonists. Platelets require a resting electrical potential across the membrane surrounding the calcium stores of greater than -70 mV in order to exhibit significant agonist-induced calcium release.

TABLE OF CONTENTS

LIST OF TABLES

LIST OF ILLUSTRATIONS

Chapter 1

Introduction

Cells interact with their environment by sensing external chemical signals through binding events at receptors on their surface. External signals are transmitted internally by a successive relay of chemical reactions occurring within the cell's cytoplasm and organelles. These chemical changes ultimately manifest in a change in the cell's phenotype or behavior. Some individual biochemical reactions in cells are relatively simple. Consider the hydrolysis of sucrose to glucose and fructose catalyzed by invertase. In this case the reaction can be fully characterized by a Michaelis-Menten relationship and a few fixed parameters. However there are many such reactions occurring simultaneously within cells and even just a few nonlinear interactions can produce complex and completely counterintuitive behavior. An example is the "chemical clock" Belousov-Zhabotinsky reaction where just a few reactants will spontaneously form numerous pulsing, spiraling waves of oscillating color until the reactants are consumed [1]. Another would be the complex, unique fractal structures of snowflakes forming from crystallizing water droplets. These are examples of the phenomenon of *emergence*, or

how complex behaviors arise from relatively simple interactions. In biology, nonlinear chemical or physical couplings among biomolecules, inorganic ions and other compounds allow cells to function as biochemical systems which are far greater than the sum of their parts.

Some examples of emergent behavior in biology include

- **Cell differentiation during development.** A central question in developmental biology is how groups of precursor cells can selectively differentiate to form organs. Using the *Drosophila* fruit fly as a model, many seminal studies revealed such patterned development arises from concentration gradients of morphogenic compounds. These gradients are the consequence of directed transport through the tissue, or nondirectional secretion from cells. Through binding and activating cell surface receptors, the morphogens themselves can affect the rate of secretion, creating a feedback loop reliant on intracellular kinetics and processes [2].
- **Spread of infectious disease.** The spread of pathogens through a population is strongly influenced by the rate of propagation of the disease between organisms. These rates are affected by population factors such as environment or demographics and individual factors like behavior and health. At the molecular biology level, acquired immunity or resistance, and genetic immune disorders also affect transmission. With the increasing amount of demographic data available, agent based modeling finds utility in incorporating data on average individual's daily activities, social interactions, and travels to develop models that allow agencies such as the CDC to anticipate risk of contagion of new pathogens.

- **Thrombus formation in damaged blood vessels.** Thrombus formation involves chemical reactions in the flowing blood occurring in response to exposed compounds in the damaged vessel wall to generate thrombin, and activation of rolling or captured platelets by thrombin and collagen on the endothelium via outside-in cell signaling. Activated platelets can aggregate at the wound site using fibrin, which is generated by thrombin, as a scaffold. Platelets also release agonists to cause autocrine and paracrine signaling and can serve as a substrate for thrombin generation. These interactions make thrombosis a truly multiscale process resulting from complex interactions at the molecular to the cellular level.

Molecular biology is often reductionist in nature. The goal of systems biology is to integrate individual complex cell signaling mechanisms to predict emergent behavior at the cellular, tissue, or organismal scale[1]. As both the quantity of biological data and available computing power increase at exponential rates, computational models become a natural tool for this purpose. The most common computational approach taken is to use networks of ordinary differential equations to model the interactions of every reactant in a detailed manner; techniques such as molecular dynamics can be useful in providing information about individual components in these networks [3].

This thesis focuses on the application of these holistic modeling approaches to intracellular signaling in one biological system in particular - human platelets. These cells play important roles in cessation of blood flow and wound healing following injury as well as in cardiovascular diseases. The major objective of this work is to model how the

[1] Our discussion is limited to how metabolic or genomic reactions integrate at the cellular level however this concept can readily be extended to how cells integrate to form tissues and organs, which in turn interact to form entire organisms.

platelet responds to chemical agonists generated during blood clot formation. Chapter 2 shows how a previously developed bottom-up model of G-protein coupled receptor mediated calcium regulation was extended to include mechanisms for calcium influx from the extracellular space. In Chapter 3, a dense Monte Carlo sampling is applied to a physiologically constrained initial condition and parameter search space to reveal how the programmed topology (i.e. the reaction network) affects the model's preferred resting states. These resting configurations are then characterized based on their cytosolic calcium responses to a transient stimulatory input. The remainder of this chapter will provide background on the biology and clinical relevance of platelets (Section 1.1), a brief introduction to the systems biology modeling paradigm (Section 1.2), an overview of some previous platelet calcium signaling modeling work (Section 1.3) and end with a discussion and overview of store-operated calcium entry (Section 1.4), the extracellular calcium entry mechanism that we seek to model.

1.1 Platelets: Biology and Significance

Platelets are critical mediators of hemostasis, the process of stopping blood loss following injury to a blood vessel. The blood is a complex fluid environment consisting of red blood cells, white blood cells, and platelets; the noncellular portion of blood, plasma, is a complex chemical cocktail of ions and proteins. Platelets must be able to precisely respond to chemical or physical signals and changes in this environment to initiate thrombosis, the process of blood clot formation, while being robust to small stochastic changes so as not to activate at inappropriate times (e.g. in the absence of an actual injury). Dysregulation or diseases such as atherosclerosis can result in pathological

thrombus formation and embolism, which is the process where a blood clot breaks loose from the blood vessel wall and travels through the bloodstream. When these dislodged blood clots occlude a coronary artery or cerebral blood vessel, they can lead to myocardial infarction or ischemic stroke, respectively. Approximately one American every minute will die of a coronary event, and coronary heart disease alone was responsible for about 1 of every 6 deaths in the United States in 2009 [4].

The internal signaling machinery of platelets allows them to rapidly respond to changes in their external environment. Platelets do not adhere to an intact vessel wall, termed the endothelium, in healthy individuals. Following injury to the endothelium, platelets traveling through the bloodstream can be captured by exposed collagen mediated by glycoprotein Ib and von Willebrand factor (vWF) multimers. These interactions result in a platelet monolayer at the wound site, however this monolayer is insufficient to fully stop bleeding [5].

Extension of a thrombus beyond an initial platelet monolayer is heavily dependent on platelet-platelet interactions which use fibrin and fibrinogen as a bridge. Recruitment of additional platelets at this stage is strongly potentiated by local action of agonists such as ADP or thromboxane A2 (TxA_2) which activated platelets release from their storage granules, and the action of thrombin, a serine protease in the bloodstream which is initially generated at the injury site following exposure of tissue factor on the damaged endothelium. These three agonists function by binding to G-protein coupled receptors (GPCRs) on the platelet surface, activating phospholipase C β which in turn cleaves inositol 1,4,5-trisphosphate (IP_3) from membrane-bound phosphatidylinositol 4,5-bisphosphate (PIP_2). IP_3 triggers Ca^{2+} release from the intracellular Ca^{2+} stores [6],

causing Ca^{2+} in the cytosol to rise from resting levels of ~100 nM to as high as 1 μM [7]. Collagen itself also causes Ca^{2+} elevation by signaling through the tyrosine kinase GPVI; this avenue to Ca^{2+} release is particularly important as the first monolayer of platelets deposits at the wound site during clot initiation [8].

A rise in cytosolic Ca^{2+} has important downstream effects responsible for changing the platelet's phenotype to one which is able to participate in and effect the further extension of a thrombus. Ca^{2+} mediates Rap1B via Cal-DAG GEF (Ca^{2+} and diacylglycerol dependent guanine nucleotide exchange protein) [9] which is a precursor to integrin αIIbβ3 activation; this integrin binds to fibrin and fibrinogen and so functions to link platelets to one another during thrombus extension. Ca^{2+} drives shape change and spreading at the wound site via activation of myosin light chain kinase which allows for reorganization of the cytoskeleton [10, 11]. Platelets store agonists such as serotonin, ADP, and TxA_2 in storage granules [12][2] which are released into the extracellular space following Ca^{2+} elevation [13, 14]; this leads to localized autocrine and paracrine signaling events to further drive platelet aggregation. Active platelets expose phosphatidylserine (PS) on their outer plasma membrane leaflet in a Ca^{2+} and caspase dependent manner [15]. This causes the platelet's surface to take on a negative charge and be able to serve as a substrate for thrombin generation.

Platelet signaling defects can lead to bleeding diatheses or pathological thrombus formation. Dysfunctional calcium signaling can lead to pathological thrombus formation [16] and has also been linked to diabetes [17, 18] and hypertension [19]. Defects or

[2] Platelet α-granules contain numerous other factors including mediators of hemostasis (factor V, fibrinogen) but also mediators of angiogenesis (VEGF, PDGF) and cytokines, causing platelets to play important roles in angiogenesis and inflammation.

mutations in genes encoding G-protein subunits can lead to impaired platelet aggregation and prolonged bleeding times [20, 21]. These examples underlie the importance of proper platelet intracellular signaling in thrombosis.

Platelets act as an ideal system for initial model development primarily due to their simplicity and availability. Platelets lack a nucleus [22], removing the need to consider the milieu of transcriptional regulation pathways that are present in the most other cell types. Platelets are also readily available from healthy donors or patients exhibiting a particular disease of interest. Many cellular regulatory mechanisms are highly conserved in biology so that conclusions or predictions drawn from a working model are often readily extensible to other cell types. An accurate model of platelet activation also has significance on its own as a predictor of physiologic hemostasis and pathophysiologic thrombosis.

The signaling cascades involved in the platelet activation process are complex at both the extracellular and intracellular level. But, as has been seen in many other biological signaling networks, calcium plays a large role in intracellular signaling and is involved in a host of critical biological processes [23], frequently serving as the focal point of a signaling network diagram and thusly represents a natural starting point for a systems model of platelet metabolism.

1.2 Systems Biology

Cellular systems are incredibly complex with numerous, often competing reactions occurring simultaneously. Systems biology bridges the junction between mathematics and biology by applying mathematical modeling techniques to make

quantitative predictions about a system's overall behavior or derive new insights into how subcomponents of a system interact. As an example, one of the most well studied phenomena in this field has been *E. Coli* chemotaxsis which is governed by relatively few proteins whose interactions have been well characterized [24]. In fact, the understanding of bacterial chemotaxis has been so well developed that the field has turned to population modeling. For example, Korobkova et al. [25] combined experimental measurements and a simple two-state chemoreceptor model [26] to show that some of the parameters in the chemotactic sensory system are fixed in such a manner that a bacterial population can respond to chemical signals stochastically and nonuniformly, and that this type of response has survival value to the group of cells as a whole.

Much work has also been done on modeling transport into and out of the cell nucleus via the nuclear pore complex (NPC). A gradient across the nuclear membrane of RanGTP mediates the specificity of importin and exportin proteins which regulate the actual transport of compounds through NPCs. This work spanned several groups and involved several model variants of increasing complexity. The earliest model used Michaelis-Menten kinetics to simplify several multistep reactions [27]. The next variant removed the Michaelis-Menten simplifications but only characterized transport by the RanGTP gradient rather than explicitly modeling fluxes through the carrier proteins [28]. Eventually a more detailed model coupling the RanGTP gradient to the importin system [29] revealed that the Ran guanine-nucleotide exchange factor (RanGEF), the protein responsible for converting RanGDP to RanGTP, is not the limiting factor and the concentration of Ran and other molecules may be more important, settling a point of

contention between the prior model variants and revealing to experimentalists which parameters and species are the best candidates to explore with greater accuracy in the laboratory. This example illustrates value of more complex models and the collaborative and sequential nature of model building where models take on greater detail between generations. Standard model interfaces such as the Systems Biology Markup Language (SBML) [30] have been developed to facilitate model sharing between groups and the stepwise process of model development. Subcomponents of cellular machinery separated on the basis of function, like glycolysis or DNA replication are frequently developed as distinct computational modules which can serve as parts with which to assemble full integrative models of cell behavior [31].

Common approaches to modeling cell signaling typically rely on coupled systems of ordinary differential equations (ODEs) [32, 33] when the cell can be considered a well-mixed chemical reactor (often broken into subcellular compartments representing different organelles). Each ODE represents the sum of all rates of change of an individual cellular component which could be a divalent cation like Ca^{2+} or an enzyme such as DNA ligase. The nuclear transport models discussed above were based on coupled ODEs. ODE systems have the natural benefit of mechanistic detail and are particularly well suited to the study of systems where kinetic data is available for all state variables and components under study; these systems can be modeled either deterministically or stochastically [34] depending on the length scales under consideration. ODE networks have been used to model GPCR dynamics [35], epidermal growth factor stimulation of mitogen-associated kinsases [36], regulation of the cell cycle and budding in fission yeast [37, 38], and phosphoinositide and Ca^{2+} regulation in human platelets. A multicellular ODE model of

pancreatic beta cells, using stochastic modeling of K^+ channels, revealed insulin bursting in as an emergent phenomena resulting from electrical coupling of individual cells [39].

ODEs are by no means the only methods available to systems biologist. When a sufficient level of topological detail is not available to design a full mechanistic model, data-driven approaches such as clustering methods, principal components analysis, or partial least squares regression can be used to derive insight about a system when large enough datasets are available [40]. Bayesian network analysis [41] can be used to draw correlations between signaling components, in doing so perhaps directing new avenues of discovery. One group has used this technique on multivariate flow cytometry data to make causal predictions of signaling molecule interactions [42]. Neural networks have been used to incorporate topological and time dependent features of human platelet calcium signaling to accurately predict responses of platelets simultaneous application of multiple chemical agonists [43] and have been incorporated into multiscale flow models of platelet aggregation [44].

Often the emergent or complex system behavior is actually the part of the system which is experimentally observable. The most relevant example is how the intracellular calcium concentration, a complex function of the concerted action of channels, pumps, or buffering agents in cells such as platelets can be quantified by labeling the cells with a fluorescent, calcium-sensitive dye. In this case the system biologist's task is to estimate unknown mechanisms or parameters in the system using the available kinetic and mechanistic data as a benchmark or guide. This is the "inverse" problem of engineering new interactions, estimating unknown parameters or reparameterizing measured parameters whose effective values may be different in the integrated system [45]; often

this process must be performed with noisy or incomplete datasets. Global techniques for parameter estimation and validation which are applied to systems of ODEs or differential-algebraic equations include particle swarm [46], simulated annealing [47], and genetic algorithms [48, 49].

Of course, either due to computational limitations or lack of complete datasets, modeling cells' entire metabolic states is not feasible. Basic understanding derived from experiments performed on the system of interest and some biological intuition are necessary for choosing the most important components to model. To deal with large and computationally intractable or non-identifiable models, reduction techniques such as sensitivity analysis [50-52] to determine the species or parameters having the greatest effects on model outputs, or the time-scale arguments [53] to make simplifying assumptions can be employed to reduce model size.

Finally, it is important to note the value of integrative, mechanistic or bottom-up models which have been validated against experimental results is not just to recapitulate previously observed phenomena, but also to indentify new, experimentally verifiable hypotheses and thereby make manifest new avenues for research and discovery [33, 40]. Complicated, fine-grained cellular models which can reproduce experimentally measured behavior approach the pinnacle of becoming reflections of an actual cell. Modelers can exert precise control over every aspect of these virtual cells; one can easily probe the effects small changes made to one component may have on other components of the model, something which may be very difficult to do in live cells. Models can also be used to discern new candidate signaling pathways for pharmacological treatment, to estimate the efficacy of existing drugs [54], or to predict potential off-target effects. These are

particularly practical applications considering the high cost of drug discovery and development which has been estimated to cost upwards of $1.8 billion USD per drug after accounting for cost of capital [55].

1.3 Previous work in modeling platelet intracellular signaling

There are only a few current examples of platelet signaling models in the literature. One group has modeled thrombin stimulation of calcium release through PAR1, as well as downstream activation of Akt, PKC, CalDAG-GEF, $\alpha 2b\beta 3$, and dense granule release [56] using ODEs. Purvis et al. [57] developed another ODE model of IP_3-mediated Ca^{2+} release stimulated by ADP binding the $P2Y_1$ receptor. This large network of over 70 species was calibrated [58] by breaking the overall model down into functionally distinct modules [31], scanning each module's initial condition space for configurations satisfying physiologically derived homeostasis constraints, and then combining each set of solutions into a global initial condition space for the entire system. The model was also required to be responsive to $P2Y_1$ stimulation. The full model was able to accurately predict: 1.) steady-state resting concentrations for intracellular Ca^{2+}, IP_3, diacylglycerol, and phosphoinositides. 2.) intracellular Ca^{2+} transients following stimulation with doses of ADP, and 3.) the relative volume of the platelet dense tubular system.

Other modeling approaches in platelets are phenomenological rather than mechanistic. One data-driven approach has used neural networks to model the response of calcium over time to multiple stimuli [43]; another group has modeled the action of

sodium-calcium exchangers and store-operated calcium entry using very coarse-grained diffusive mass transfer equations for the transport activity of key calcium channels and pumps [59]. Such procedures can be very efficient for developing a model which yields a desired output as they require less knowledge about the underlying reaction topology, but as they lack molecular detail they are less useful for making novel predictions about the interactions among system subcomponents.

1.4 Store-operated calcium entry

Store-operated calcium entry (SOCE) is a ubiquitous mechanism that enables Ca^{2+} influx into cells from the extracellular fluid, operates in response to Ca^{2+} store depletion, and terminates as stores refill [60]. SOCE acts synergistically with Ca^{2+} release from stores to elevate cytosolic Ca^{2+} as well as to allow stores to refill. Most commonly, store depletion is the result of surface receptor activation leading to IP_3 production and activation of IP_3 receptor (IP_3R) Ca^{2+} channels in the endoplasmic reticulum (ER) membrane (the dense tubular system or DTS is the ER equivalent in platelets). The phenomenon of store-induced Ca^{2+} influx was first observed many years ago [61], but the molecular mechanisms for the process have only more recently begun to be elucidated. Irreversible SERCA inhibitors such as thapsigargin (TG) which can deplete stores independently of receptor activation have been instrumental in studying SOCE and led to the discovery of this type of current in many cell types [60], which many groups have dubbed "Ca^{2+} release-activated Ca^{2+} current" (CRAC).

Some of the hallmark characteristics of store-operated channels (SOCs), apart from their unique feature of being regulated by state of the cell's Ca^{2+} stores, are 1.) high selectivity for Ca^{2+} [62], 2.) high single channel open probability [63], and 3.) low single-channel conductance [62, 64]. The Ca^{2+} current through active SOCs is commonly abbreviated I_{SOC}. siRNA screenings for SOCE inhibitors in HeLa cells led to the identification of the transmembrane protein STIM1 in 2005 as the calcium sensor responsible for regulating SOC opening [65]. Embedded in the ER membrane, it contains a luminal facing EF-hand domain for which Ca^{2+} serves as a ligand. Loss of bound calcium results in self-association and translocation of STIM1 to regions of the cell where the ER membrane and plasma membrane (PM) are in close contact [66-69]. These aggregates of STIM1 close to the PM are called puncta. Mutations of the EF-hand domain of STIM1 result in constitutive puncta formation and SOCE channel activation [65, 66, 70]. STIM1's Ca^{2+} affinity has been measured to be between 200 – 600 μM [71]. Forster resonance energy transfer (FRET) studies have shown STIM1 oligomerizes prior to puncta entry [69]. About a year following the initial discovery of STIM1, additional siRNA screens in *Drosophila* cells revealed the Orai1 protein[3] as being the actual channel pore-forming subunit in the plasma membrane [73-75]. Mammalian cells possess genes for two additional variants of Orai [76]. Of these three, Orai1 is the most likely candidate as the mediator of CRAC on the basis that loss of function mutations in T cells [73] and mouse platelets [77] largely abolishes SOCE. Orai1 accumulates in puncta over similar time scales as STIM1 [78].

[3] The gene Orai derives its name from Greek mythology where the Orai are the three keepers of the gates of heaven: Eunomia (Order, Harmony), Dike (Justice), and Eirene (Peace) 72. Homer, R. Fagles, and B. Knox, *The Iliad*. 1990, New York, N.Y., U.S.A.: Viking. xvi, 683 p.

More recent publications have studied the molecular interactions between STIM1 and Orai1. Orai1 has its N and C termini facing the cytosol [79-81]; STIM1 can interact with both of these domains via its so called Stim-Orai Activating Region (SOAR) in order to gate the channel [82, 83]. Channel opening occurs in a graded fashion as a function of the number of STIM1 dimers bound; maximal channel activation requires a stoichiometry of 4 STIM1 dimers per tetrameric Orai1 complex [84, 85]. High levels of Orai1 expression can actually reduce I_{SOC} [66, 86-88], possibly be decreasing the ratio of STIM1:Orai1 and thereby lowering the average channel open probability [85]. Figure 1.1 illustrates the general process of SOCE activation.

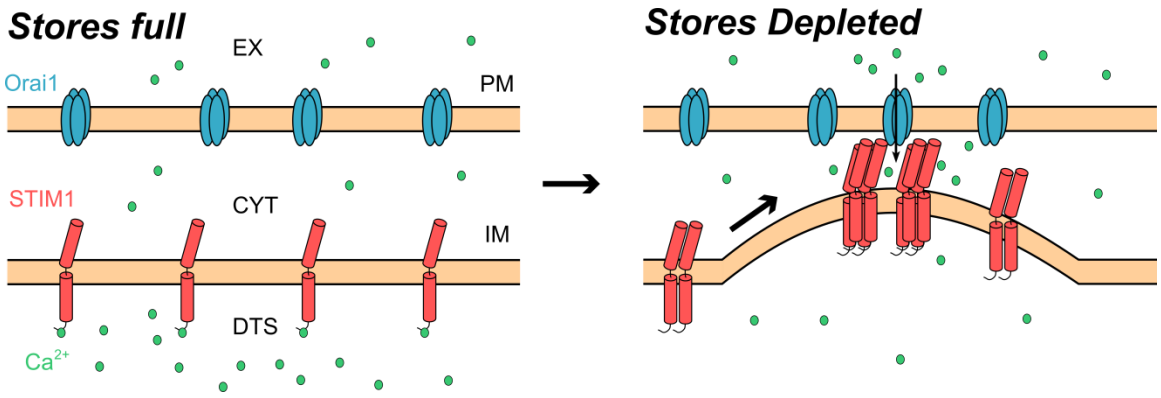

Figure 1.1 Mechanism for store-operated calcium entry activation.

In a resting cell, STIM1 and Orai1 are dispersed throughout their respective membranes (left). Following store depletion, STIM1 loses its bound Ca^{2+} ligand (right), self-associates to form dimers, colocalizes with Orai1 at sites of inner membrane and plasma membrane contact where it can initiate channel opening. Abbreviations: EX: extracellular space; PM: plasma membrane; CYT: cytosol; IM: inner membrane; DTS, dense tubular system, the Ca^{2+} stores of platelets.

Many studies have shown SOCE playing a direct role in physiologic and pathophysiologic processes including metastasis [89], endothelial proliferation [90] and muscle cell contraction and motility [91-93]. In the context of platelets and thrombosis, mouse platelets lacking STIM1 and Orai1 showed reduced Ca^{2+} response to collagen and thrombin and impaired thrombus formation *in vitro* flow systems [16, 77, 94]. SOCE also has been shown to be required for PS exposure in agonist-stimulated human platelets [95]. Ca^{2+} entry through Orai1 has been shown to induce primary keratinocytes in the basal epidermis to proliferate and migrate while inhibiting terminal differentiation [96]. Interestingly, $STIM1^{-/-}$ mouse platelets show normal αIIbβ3 activation, aggregation and degranulation through GPCR-induced store depletion. STIM1 and Orai1 knockout had a cardioprotective effect in mouse models of arterial thrombosis and ischemic brain infarction while being associated with only mildly prolonged bleeding times [77]. This evidence may suggest that in platelets SOCE may play a role in events following the early events of thrombosis such as thrombus stabilization or clot retraction [97].

So far no group has modeled the complete process for store-operated calcium entry outlined in Figure 1.1 with mechanistic detail in any cell type. A central portion of the work in this thesis has been to integrate the current understanding of SOCE into a previously published model of IP_3 mediated calcium release in platelets [57].

Chapter 2

Model Construction

The regulation of intracellular calcium is essential to numerous cellular processes. During hemostasis, platelets maintain a low resting intracellular cytoplasmic calcium concentration ($[Ca^{2+}]_{cyt}$) as they transit through healthy vessels, yet rapidly activate and mobilize $[Ca^{2+}]_{cyt}$ to stop bleeding at injury sites. Platelet $[Ca^{2+}]_{cyt}$ mobilization is associated with integrin activation, dense (δ) and α-granule release, thromboxane A_2 synthesis, shape change, and phosphatidylserine exposure. Receptor-mediated signaling through the collagen receptor (GPVI), ADP receptor ($P2Y_1$), thromboxane A_2 receptor (TP), and thrombin receptors (PAR1 and PAR4 in human platelets) results in inositol [1,4,5]-trisphosphate (IP_3)-mediated calcium release from the dense tubular system (DTS) via IP_3-receptor (IP_3R) activation. The DTS transmembrane protein stromal interaction molecule 1 (STIM1) becomes activated as DTS calcium ($[Ca^{2+}]_{dts}$) drops, resulting in formation of clusters of STIM1-Orai complexes as the DTS membrane forms a punctate association with the plasmalemma membrane (PM) containing Orai1. The STIM1-Orai1 complexes mediate store-operated calcium entry (SOCE) to enhance the

activation state of the cell. Platelets deficient in SOCE show reduced response to agonist-induced stimulation and impaired thrombus growth and stability under flow [77]. Following stimulus, $[Ca^{2+}]_{cyt}$ is then returned to near-resting levels by the action of two ATP-dependent pumps, the plasma membrane and sarco/endoplasmic reticulum Ca^{2+}-ATPase's (PMCA and SERCA). The SERCA is responsible for DTS refilling.

A systems biology approach to quantify platelet homeostasis and activation must consider diverse molecular mechanisms that act in concert to regulate intracellular calcium. Platelets are an excellent tool for signal transduction studies: they are routinely available from human donors, lack a genome (obviating the need to predict gene regulation), are amenable to high throughput experiments, and present numerous druggable targets. The molecular components of calcium regulation in the platelet include IP_3R, SERCA, calmodulin-regulated PMCA, puncta formation, and STIM1-Orai (Figure 2.1), components that are also well represented in many other cell types. An accurate model of platelet activation may help predict hemostasis, thrombosis, or drug response.

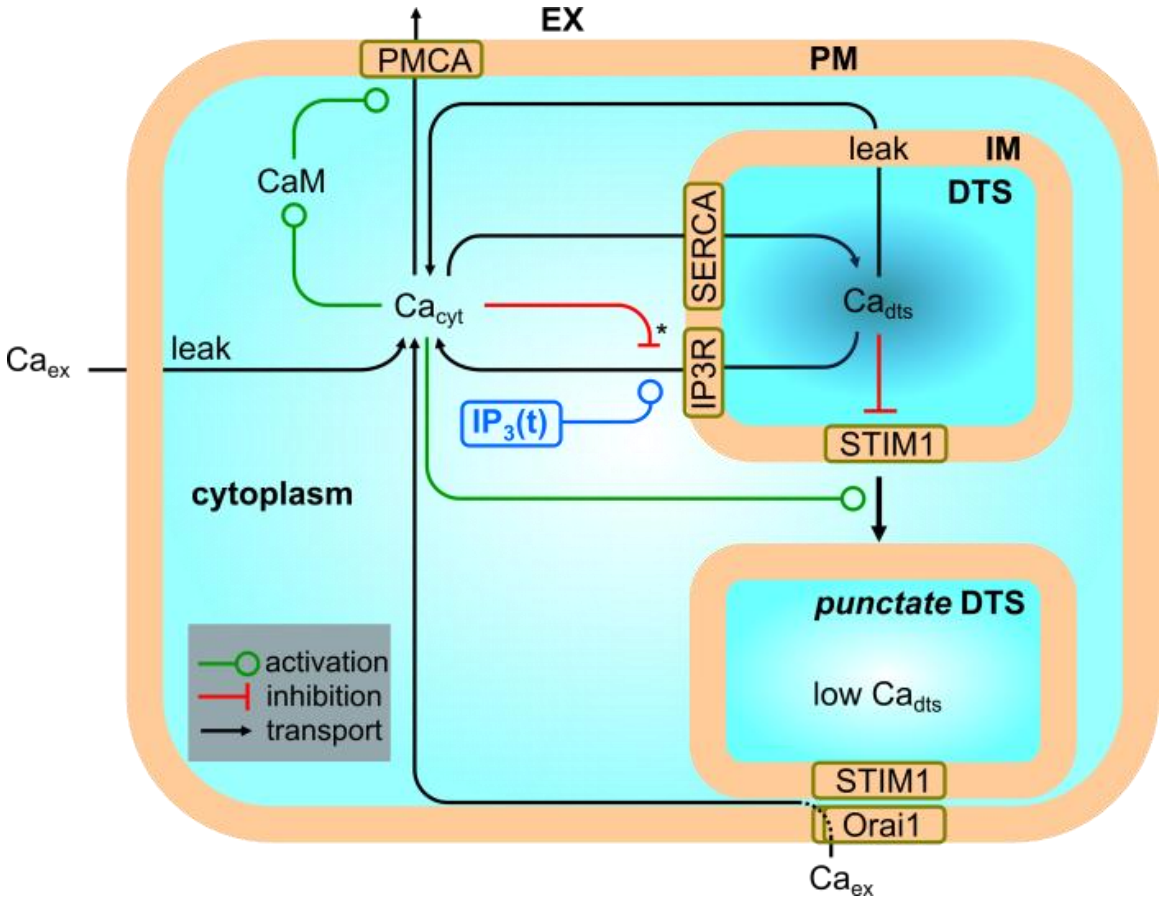

Figure 2.1 Overall model topology.

The full model is comprised of 34 species, 35 reactions, 86 parameters and 5 compartments. Three dimensional compartments are: extracellular (EX), dense-tubular system (DTS) and the cytoplasm. Two dimensional compartments are the DTS inner membrane (IM) and the plasma membrane (PM). $[Ca^{2+}]_{cyt}$ has a biphasic influence on IP_3R activity; it stimulates IP_3R at lower concentrations and becomes inhibitory at high concentrations. $[Ca^{2+}]_{cyt}$ is also defined as a regulator of puncta formation. The system is activated by IP_3 (blue) which is explicitly controlled as a function of time with exponential or piecewise polynomial forcing functions.

In a prior bottom-up ODE model [57, 58], GPCR signaling through $P2Y_1$ activation by ADP was combined with $G\alpha_q$ activation of phospholipase-C_β, phosphoinositide metabolism, PKC activation, and calcium release by IP_3 and reuptake by the SERCA pump. With 132 fixed kinetic parameters taken from the literature, this model topology accurately predicted population and single cell dynamics in the absence of extracellular calcium influx (as in experiments employing extracellular EDTA). Central to finding allowable initial conditions for unknown species concentrations, the *homeostasis assumption* requires the initial condition to be a steady state solution with low resting $[Ca^{2+}]_{cyt}$ that also allows responsiveness to elevated IP_3. The work presented in this and the next Chapter [98] extends this model by allowing for external calcium entry.

Calcium entry from the extracellular environment is important for sustained platelet activation. The present study considers the regulation of calcium flux across the plasma membrane by store-operated channels (SOCs), which are a calcium channel found in many excitable and non-excitable cell types [60]. The defining characteristics of SOCs are: low single channel conductance, high open probability, and high selectivity for calcium [60]. Known platelet copy number for many of the key constituents [99] provided a starting point for a high dimensional exploration of the model's behavior. The model accurately predicted stable resting $[Ca^{2+}]_{cyt}$ and $[Ca^{2+}]_{dts}$ as well as IP_3-triggered calcium mobilization in both calcium-containing and calcium-free (EDTA) extracellular buffer. Additionally, the dynamics of DTS membrane-plasmalemma puncta formation during activation (as a prerequisite for SOCE) was essential to predicting appropriate platelet characteristics in the presence of extracellular calcium ($[Ca^{2+}]_{ex}$).

2.1 Model Construction and Simulation

The set of reactions describing the model topology (see Figure 2.1 and Figure 2.2 and Table 2.1) were modeled as a coupled set of ordinary differential equations (ODEs) spanning five compartments. For a system with n state variables the governing equations can be represented as

$$\frac{d\boldsymbol{c}}{dt} = \boldsymbol{f}(t) = \begin{bmatrix} f_1(\boldsymbol{c}) \\ f_2(\boldsymbol{c}) \\ \vdots \\ f_n(\boldsymbol{c}) \end{bmatrix};\ \boldsymbol{c}(t_0) = \boldsymbol{c_0} \tag{2.1}$$

Each element f_i is the sum of all reactions or transport equations which produce, consume or transport state *i*. For reactions occurring at compartmental interfaces, concentrations of species in a two dimensional compartment were scaled to the bulk (three dimensional) compartment following the procedure described by Kholodenko et al. [100]. Each compartment was assumed to be well mixed on the basis of the platelet's small volume (< 10 fL) [101]. Except for specific cases discussed in sections to follow, reactions were modeled with either mass action kinetics or kinetics similar to Michaelis-Menten. Model simulations were performed using the SBToolBox2 software package add-on for MATLAB (The MathWorks, Natick, MA) [102].

2.2 Model Overview

The calcium model (see Figure 2.1) comprises five compartments: the extracellular space (EX), cytosol (CYT) and dense tubular system (DTS) which are separated by the plasma membrane (PM) and DTS inner membrane (IM). Calcium is kept

in balance by four major processes which can be separated into kinetically distinct submodules shown in Figure 2.2, *A–D*. In the resting platelet, a low intracellular calcium concentration ($[Ca^{2+}]_{cyt}$) is maintained by the action of Ca^{2+} ATPases in the PM and IM. The calmodulin (CaM) dependent Ca^{2+} transporter PMCA (Figure 2.2 *C*) pumps calcium into the EX and SERCA (Figure 2.2 *A*) pumps Ca^{2+} across the IM into the DTS.

	Reaction / Quantity	Mechanism	Rate Law / Rule	Parameter Values	Ref.
SERCA	**SERCA shuttling**	$SERCA_{E2} \leftrightarrow SERCA_{E1}$	$k_1 \cdot [SERCA_{E2}] - k_{-1} \cdot [SERCA_{E1}]$	k_1 = 600 s^{-1}, k_{-1} = 600 s^{-1}	1
SERCA	**Ca^{2+}_{cyt} binding SERCA**	$SERCA_{E1} + 2\ Ca^{2+}_{cyt} \leftrightarrow SERCA_{E1}{\cdot}Ca^{2+}$	$k_1 \cdot [SERCA_{E1}] \cdot [Ca^{2+}_{cyt}] \cdot [Ca^{2+}_{cyt}] - k_{-1} \cdot [SERCA_{E1}{\cdot}Ca^{2+}]$	k_1 = 1 × 10^{15} $M^{-2}{\cdot}s^{-1}$, k_{-1} = 10 s^{-1}	1
SERCA	**Phosphorylation of SERCA**	$SERCA_{E1}{\cdot}Ca^{2+} \leftrightarrow SERCA_{E1}P{\cdot}Ca^{2+}$	$k_1 \cdot [SERCA_{E1}Ca^{2+}] - k_{-1} \cdot [SERCA_{E1}P{\cdot}Ca^{2+}]$	k_1 = 700 s^{-1}, k_{-1} = 5 s^{-1}	1
SERCA	**Ca^{2+} transport across IM**	$SERCA_{E1}P{\cdot}Ca^{2+} \leftrightarrow SERCA_{E2}P{\cdot}Ca^{2+}$	$k_1 \cdot [SERCA_{E1}P{\cdot}Ca^{2+}] - k_{-1} \cdot [SERCA_{E2}P{\cdot}Ca^{2+}]$	k_1 = 600 s^{-1}, k_{-1} = 50 s^{-1}	1
SERCA	**Ca^{2+}_{dts} release into DTS**	$SERCA_{E2}P{\cdot}Ca^{2+} \leftrightarrow SERCA_{E2}P + 2\ Ca^{2+}_{dts}$	$k_1 \cdot [SERCA_{E2}P{\cdot}Ca^{2+}] - k_{-1} \cdot [SERCA_{E2}P] \cdot [Ca^{2+}_{dts}] \cdot [Ca^{2+}_{dts}]$	k_1 = 1000 s^{-1}, k_{-1} = 4 × 10^9 $M^{-2}{\cdot}s^{-1}$	1
SERCA	**SERCA dephosphorylation**	$SERCA_{E2}P \leftrightarrow SERCA_{E2}$	$k_1 \cdot [SERCA_{E2}P] - k_{-1} \cdot [SERCA_{E2}]$	k_1 = 500 s^{-1}, k_{-1} = 1 s^{-1}	1
IP_3R	**IP_3R inhibition**	$IP_3R_n + Ca^{2+}_{cyt} \leftrightarrow IP_3R_{I1}$	$[IP_3R_n] \cdot ((k_1 \cdot L_1 + I_2) \cdot [Ca^{2+}_{cyt}] / (L_1 + [Ca^{2+}_{cyt}] \cdot (1 + L_1 / L_3)))$	k_1 = 0.64 $s^{-1}{\cdot}\mu M^{-1}$, L_1 = 0.12 μM, I_2 = 1.7 s^{-1}	2
IP_3R			$- [IP_3R_{I1}] \cdot (k_{-1} + I_{-2})$	L_3 = 0.025 μM, k_{-1} = 0.04 s^{-1}, I_{-2} = 0.8 s^{-1}	
IP_3R	**IP_3R binding IP_3**	$IP_3R_n + IP_3 \leftrightarrow IP_3R_o$	$[IP_3R_n] \cdot [IP_3] \cdot ((k_2 \cdot L_3 + I_4 \cdot [Ca^{2+}_{cyt}]) / (L_3 + [Ca^{2+}_{cyt}] \cdot (1 + L_3 / L_1)))$	k_2 = 37.4 $s^{-1}{\cdot}\mu M^{-1}$, I_4 = 1.7 $s^{-1}{\cdot}\mu M^{-1}$	2
IP_3R			$- [IP_3R_o] \cdot ((k_{-2} + I_{-4} \cdot [Ca^{2+}_{cyt}]) / (1 + [Ca^{2+}_{cyt}] / L_5))$	k_{-2} = 1.4 s^{-1}, I_{-4} = 2.5 $\mu M^{-1}{\cdot}s^{-1}$, L_5 = 54.7 μM	
IP_3R	**IP_3R activation**	$IP_3R_o + Ca^{2+}_{cyt} \leftrightarrow IP_3R_a$	$[IP_3R_o] \cdot ((k_4 \cdot L_5 + I_6) \cdot [Ca^{2+}_{cyt}] / (L_5 + [Ca^{2+}_{cyt}]))$	k_4 = 4 $s^{-1}{\cdot}\mu M^{-1}$, I_6 = 4707 s^{-1}	2
IP_3R			$- [IP_3R_a] \cdot (L_1 \cdot (k_{-4} + I_{-6}) / (L_1 + [Ca^{2+}_{cyt}]))$	k_{-4} = 0.54 $s^{-1}{\cdot}\mu M^{-1}$, I_{-6} = 11.4 s^{-1}	2
IP_3R	**IP_3R inhibition**	$IP_3R_a + Ca^{2+}_{cyt} \leftrightarrow IP_3R_{I2}$	$[IP_3R_a] \cdot (k_1 \cdot L_1 + I_2) \cdot [Ca^{2+}_{cyt}] / (L_1 + [Ca^{2+}_{cyt}]) - [IP_3R_{I2}] \cdot (k_{-1} + I_{-2})$		2
IP_3R	**IP_3R closing**	$IP_3R_o \leftrightarrow IP_3R_s$	$[IP_3R_o] \cdot (k_{-3} \cdot L_5 / (L_5 + [Ca^{2+}_{cyt}])) - [IP_3R_s] \cdot k_{-3}$	k_{-3} = 11 $s^{-1}{\cdot}\mu M^{-1}$, k_{-3} = 29.8 s^{-1}	2
IP_3R	**Channel open probability (P_{oIP3R})**		$(0.9 \cdot IP_3R_a / IP_3R_{total} + 0.1 \cdot pIP_3R_o / IP_3R_{total})^4$		2
IP_3R	**IM potential (ψ_{IM})**		$RT / zF \cdot \ln (Ca^{2+}_{cyt} / Ca^{2+}_{dts})$		
IP_3R	**Ca^{2+} release from DTS via IP_3R**	$Ca^{2+}_{dts} \leftrightarrow Ca^{2+}_{cyt}$	$N_{IP3R} \cdot P_{oIP3R} \cdot \gamma_{IP3R} \cdot e \cdot (V_{IM} - \psi_{IM})$	γ_{IP3R} = 10 pS	3
SOCE	**Ca^{2+}_{dts} binding STIM1**	$STIM1 + Ca^{2+}_{dts} \leftrightarrow STIM1{\cdot}Ca^{2+}_{dts}$	$k_1 \cdot [STIM1] \cdot [Ca^{2+}_{dts}] - k_{-1} \cdot [STIM1{\cdot}Ca^{2+}]$	k_{-1}/k_1 = 200 μM	4
SOCE	**STIM1 dimerization**	$2\ STIM1 \leftrightarrow STIM1_2$	$k_1 \cdot [STIM1] \cdot [STIM1] - k_{-1} \cdot [STIM1_2]$	k_1 = 9 × 10^8 $s^{-1}{\cdot}M^{-1}$, k_{-1} = 3.5 s^{-1}	This study
SOCE	**Puncta formation factor (θ_p)**		$\alpha \cdot [Ca^{2+}_{cyt}]^n / ([Ca^{2+}_{cyt}]^n + K_M^n) + 0.01$	K_M = 100 - 300 nM, n = 0.5 - 3, α = 0.2	This study
SOCE	**$STIM1_2$ puncta entry ($(STIM1_2)_p$)**	$STIM1_2 \leftrightarrow (STIM1_2)_p$	$[STIM1_2] \cdot \theta_p$		
SOCE	**STIM in puncta binding Orai1**	$(STIM1_2)_p + Orai1 \leftrightarrow (STIM1_2)_p{\cdot}Orai1$	*see equations below*		
SOCE	**Orai (closed) with 1 $STIM1_2$ bound**		$4 \cdot K_a \cdot [C] \cdot [S]$	K_a = 100	5
SOCE	**Orai (closed) with 2 $STIM1_2$ bound**		$3 / 2 \cdot K_a \cdot a \cdot [CS] \cdot [S]$	a = 0.5	5
SOCE	**Orai (closed) with 3 $STIM1_2$ bound**		$2 / 3 \cdot K_a \cdot a^2 \cdot [CS_2] \cdot [S]$		5
SOCE	**Orai (closed) with 4 $STIM1_2$ bound**		$1 / 4 \cdot K_a \cdot a^3 \cdot [CS_3] \cdot [S]$		5
SOCE	**Orai (open) with 0 $STIM1_2$ bound**		$L \cdot [C]$	L = 0.0001	5
SOCE	**Orai (open) with 1 $STIM1_2$ bound**		$4 \cdot K_a \cdot f \cdot [O] \cdot [S]$	f = 1420	5
SOCE	**Orai (open) with 2 $STIM1_2$ bound**		$3 / 2 \cdot K_a \cdot f \cdot a \cdot [OS] \cdot [S]$		5
SOCE	**Orai (open) with 3 $STIM1_2$ bound**		$2 / 3 \cdot K_a \cdot f \cdot a^2 \cdot [OS_2] \cdot [S]$		5
SOCE	**Orai (open) with 4 $STIM1_2$ bound**		$1 / 4 \cdot K_a \cdot f \cdot a^3 \cdot [OS_3] \cdot [S]$		5
SOCE	**$(STIM1_2)_p$ mass balance**		$[S] + [CS] + 2 \cdot [CS_2] + 3 \cdot [CS_3] + 4 \cdot [CS_4] + [OS] + 2 \cdot [OS_2] +$		5
SOCE			$3 \cdot [OS_3] + 4 \cdot [OS_4]$		
SOCE	**Orai1 mass balance**		$[C] + [CS] + [CS_2] + [CS_3] + [CS_4] + [OS] + [OS_2] + [O] + [OS_3] + [OS_4]$		5
SOCE	**PM potential (ψ_{PM})**		$RT / zF \cdot \ln (Ca^{2+}_{ex} / Ca^{2+}_{cyt})$		
SOCE	**Calcium entry via SOC channels**	$Ca^{2+}_{ex} \rightarrow Ca^{2+}_{cyt}$	$\gamma_{SOC} \cdot e \cdot (V_{PM} - \psi_{PM}) \cdot \sum_i (OS_i)$	γ_{SOC} = 0.02 pS	5, 6
PMCA	**PMCA binding cytosolic Ca**	$Ca^{2+}_{cyt} + PMCA \leftrightarrow Ca^{2+}{\cdot}PMCA$	$k_1 \cdot [PMCA] \cdot [Ca^{2+}_{cyt}] - k_{-1} \cdot [Ca^{2+}{\cdot}PMCA]$	k_1 = 1 × 10^7 $s^{-1}{\cdot}M^{-1}$, k_{-1} = 50 s^{-1}	7
PMCA	**PMCA releasing Ca into EX**	$Ca^{2+}{\cdot}PMCA \rightarrow PMCA + Ca^{2+}_{ex}$	$k_1 \cdot [Ca^{2+}{\cdot}PMCA]$	k_1 = 5.5 s^{-1}	7
PMCA	**First two Ca^{2+}_{cyt} binding CaM**	$CaM + 2\ Ca^{2+}_{cyt} \leftrightarrow Ca^{2+}{}_2{\cdot}CaM$	$k_1 \cdot [CaM] \cdot [Ca^{2+}_{cyt}]^2 - k_{-1} \cdot [Ca^{2+}{}_2{\cdot}CaM]$	k_1 = 2.669 × 10^{12} $s^{-1}{\cdot}M^{-2}$, k_{-1} = 2.682 s^{-1}	7
PMCA	**Second two Ca^{2+}_{cyt} binding CaM**	$Ca^{2+}{}_2{\cdot}CaM + 2\ Ca^{2+}_{cyt} \leftrightarrow Ca^{2+}{}_4{\cdot}CaM$	$k_1 \cdot [CaM{\cdot}Ca^{2+}{}_2] \cdot [Ca^{2+}_{cyt}]^2 - k_{-1} \cdot [Ca^{2+}{}_4{\cdot}CaM]$	k_1 = 1.704 × 10^{14} $s^{-1}{\cdot}M^{-2}$, k_{-1} = 1.551 s^{-1}	7
PMCA	**CaM binding and activating PMCA**	$PMCA + Ca^{2+}{}_4{\cdot}CaM \leftrightarrow PMCA{\cdot}(Ca^{2+}{}_4{\cdot}CaM)$	$k_1 \cdot [CaM{\cdot}Ca^{2+}{}_4] \cdot [PMCA] - k_{-1} \cdot [PMCA{\cdot}(Ca^{2+}{}_4{\cdot}CaM)]$	k_1 = 2 × 10^5 $s^{-1}{\cdot}M^{-1}$, k_{-1} = 0.0008 s^{-1}	7
PMCA	**PMCA/CaM binding cytosolic Ca**	$PMCA{\cdot}(Ca^{2+}{}_4{\cdot}CaM) + Ca^{2+}_{cyt} \leftrightarrow$	$k_1 \cdot [PMCA{\cdot}(Ca^{2+}{}_4{\cdot}CaM)] \cdot [Ca^{2+}_{cyt}] - k_{-1} \cdot [PMCA{\cdot}(Ca^{2+}4{\cdot}CaM){\cdot}Ca^{2+}]$	k_1 = 5 × 10^7 $s^{-1}{\cdot}M^{-1}$, k_{-1} = 10 s^{-1}	7
PMCA		$PMCA{\cdot}(Ca^{2+}{}_4{\cdot}CaM){\cdot}Ca^{2+}_{cyt}$			
PMCA	**PMCA/CaM releasing Ca into EX**	$PMCA{\cdot}(Ca^{2+}{}_4{\cdot}CaM){\cdot}Ca^{2+}_{cyt} \rightarrow$	$k_1 \cdot [PMCA{\cdot}(Ca^{2+}4{\cdot}CaM){\cdot}Ca^{2+}]$	k_1 = 30 s^{-1}	7
PMCA		$PMCA{\cdot}(Ca^{2+}{}_4{\cdot}CaM) + Ca^{2+}_{ex}$			
PMCA	**Release of Ca^{2+}_{cyt} bound to CaM**	$PMCA{\cdot}(Ca^{2+}{}_4{\cdot}CaM) \leftrightarrow PMCA{\cdot}CaM + 4\ Ca^{2+}_{cyt}$	$k_1 \cdot [PMCA{\cdot}(Ca^{2+}4{\cdot}CaM)] - k_{-1} \cdot [PMCA{\cdot}CaM] \cdot [Ca^{2+}_{cyt}]^4$	k_1 = 10 s^{-1}, k_{-1} = 7.332 × 10^{20} $s^{-1}{\cdot}M^{-4}$	7
PMCA	**Dissociation of PMCA and CaM**	$PMCA{\cdot}CaM \rightarrow PMCA + CaM$	$k_1 \cdot [PMCA{\cdot}CaM]$	k_1 = 0.033 s^{-1}	7
Leak	**Calcium leak across IM**	$Ca^{2+}_{dts} \leftrightarrow Ca^{2+}_{cyt}$	$k_1 \cdot ([Ca^{2+}_{dts}] - [Ca^{2+}_{cyt}])$	k_1 = 0.003333 s^{-1}	8
Leak	**Calcium leak across PM**	$Ca^{2+}_{ex} \leftrightarrow Ca^{2+}_{cyt}$	$SA_{PM} \cdot \gamma_{leak} \cdot \psi_{PM}$	γ_{leak} = 0.7 pS·m^{-2}	9

Table 2.1 Reaction equations, rate laws, and kinetic constants.

All of the model reactions or algebraic equations are presented and grouped according to the major mechanism which they govern: SERCA, IP_3R, SOCE, or PMCA. All fixed parameters are taken from the references given in the final column and listed below. Rate constants for STIM1 dimerization and the parameters in the puncta entry Hill function equation were estimated in the present study.

Table 2.1 References

1. Dode, L., B. Vilsen, K. Van Baelen, F. Wuytack, J. D. Clausen, and J. P. Andersen. 2002. Dissection of the functional differences between sarco(endo)plasmic reticulum Ca2+-ATPase (SERCA) 1 and 3 isoforms by steady-state and transient kinetic analyses. J Biol Chem 277:45579-45591.

2. Sneyd, J., and J. F. Dufour. 2002. A dynamic model of the type-2 inositol trisphosphate receptor. Proc Natl Acad Sci U S A 99:2398-2403.

3. Alberts, B. 2002. Molecular biology of the cell. Garland Science, New York.

4. Lewis, R. S., M. M. Wu, and R. M. Luik. 2007. Some assembly required: Constructing the elementary units of store-operated Ca2+ entry. Cell Calcium 42:163-172.

5. Hoover, P. J., and R. S. Lewis. 2011. Stoichiometric requirements for trapping and gating of Ca2+ release-activated Ca2+ (CRAC) channels by stromal interaction molecule 1 (STIM1). Proc Natl Acad Sci U S A.

6. Lewis, R. S. 2011. Store-operated calcium channels: new perspectives on mechanism and function. Cold Spring Harb Perspect Biol 3.

7. Caride, A. J., A. G. Filoteo, J. T. Penniston, and E. E. Strehler. 2007. The Plasma Membrane Ca2+ Pump Isoform 4a Differs from Isoform 4b in the Mechanism of Calmodulin Binding and Activation Kinetics: Implications for Ca2+ Signaling. Journal of Biological Chemistry 282:25640-25648.

8. Juska, A. 2010. Plasma membrane calcium pump and sodium-calcium exchanger in maintenance and control of calcium concentrations in platelets. Biochem Biophys Res Commun 392:41-46.

9. Purvis, J. E., M. S. Chatterjee, L. F. Brass, and S. L. Diamond. 2008. A molecular signaling model of platelet phosphoinositide and calcium regulation during homeostasis and P2Y1 activation. Blood 112:4069-4079.

IP_3R channels (Figure 2.2 *B*) release Ca^{2+} from the DTS into the cytosol in response to a rise in $[IP_3]$. SOCs (Figure 2.2 *D*) allow calcium entry into the CYT across the PM in response to store depletion. Calcium pumping via SERCA was modeled using a kinetic study and model of the SERCA3b isoform [103] which is the most abundant isoform in platelets [99].

IP_3R kinetics are described with a six state model [104] with two active confirmations that are positively regulated by $[IP_3]$ and biphasically regulated by $[Ca^{2+}]_{cyt}$. Channel open probability (P_o) is based on the total number of tetrameric channels in either of the two active confirmations (Table 1). For PMCA transport, we use a kinetic model of PMCA 4b, an isoform abundant in platelets and erythrocytes [99, 105]. PMCA independently and irreversibly transports Ca^{2+} and if bound to CaM transports Ca^{2+} with much higher affinity and turnover rate [106, 107]. The volume of the human platelet cytosol is ~6 fL [108] and the volume of the DTS has been estimated to range from 1 – 10% of the cytosol volume by electron microscopy of glucose-6 phosphatase stained platelets[57, 109].

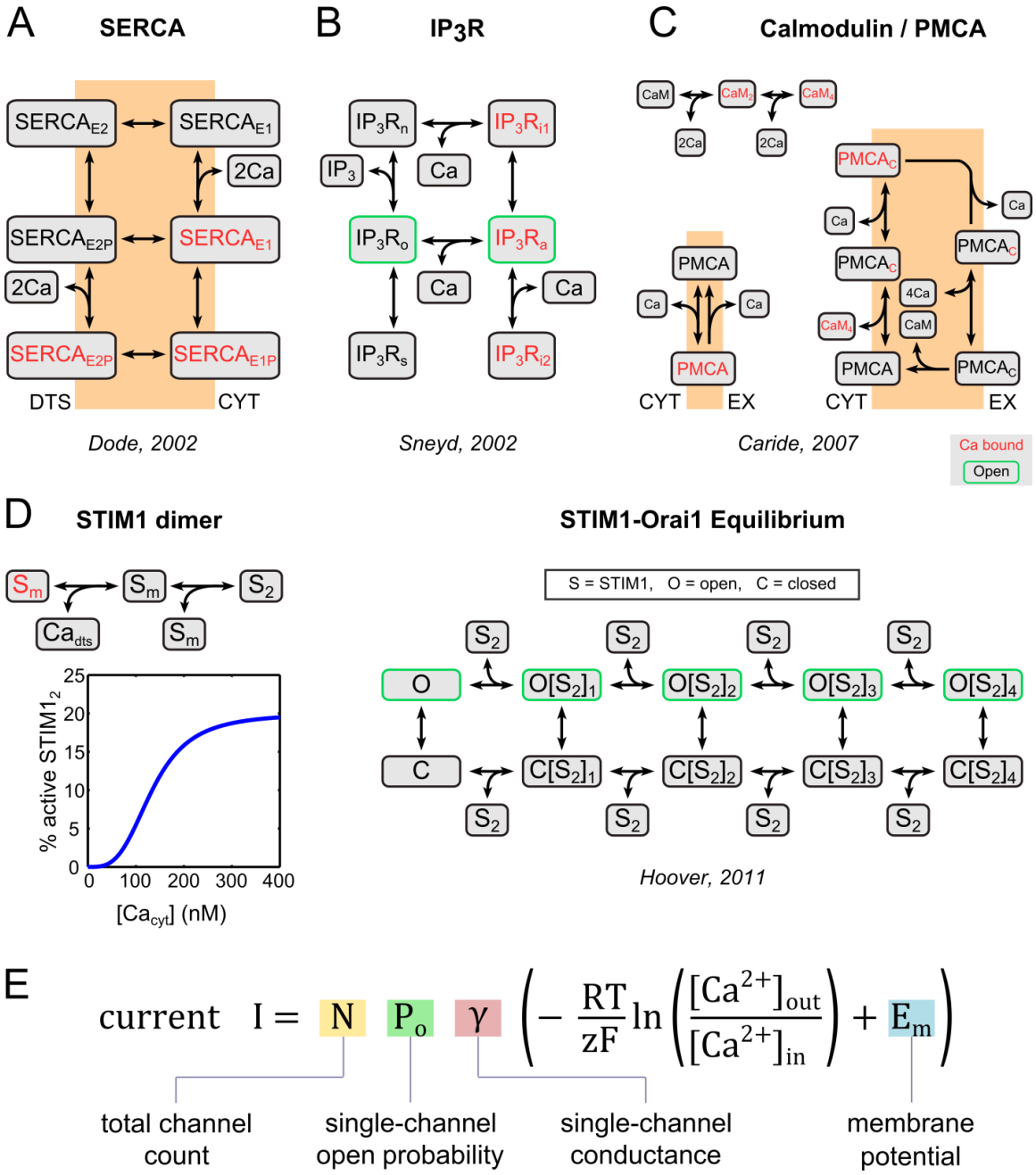

Figure 2.2 Submodule schematics and calcium current equation.

(*A*) SERCA Transport. Subscripts: E1, facing cytosol; E2, facing DTS; P, phosphorylated. (*B*) IP_3R dynamics. Subscripts: n, native; i1, inhibited; o, open; a, active; s, shut; i2, inhibited. (*C*) PMCA Transport. PMCA can irreversibly transport calcium independently (slow) or with CaM as a cofactor (fast). Subscripts: C, calmodulin bound; 2, two calcium ions bound; 4, four calcium ions bound. (*D*) SOC assembly and dynamics. Calcium dissociation results in cytosolic calcium dependent translocation of dimerized STIM to puncta. STIM in the puncta instantaneously equilibrates with Orai according to a

set of Monod-Wyman-Changeux (MWC) equilibrium relationships determined by Hoover et al. [85]. Subscripts: m, monomeric STIM; 2, dimeric STIM. (*E*) Calcium current equation. In panels *A* – *D*, an arrow with two arrowheads indicates a reversible reaction while a single arrowhead indicates an irreversible reaction. Red text indicates calcium is bound. A green outline indicates a channel is open.

2.3 Modeling ion channel current and membrane potential

The driving force across an ion channel embedded in a biological membrane is the difference between the electrical potential across the membrane (E_m) and the reversal potential of the ion which is given by the Nernst equation [110]. Net calcium current is therefore given by Eq. (2.2):

$$I = \gamma N P_0 \frac{N_A}{F}\left(-\frac{RT}{zF}\ln\left(\frac{[Ca^{2+}_{out}]}{[Ca^{2+}_{in}]}\right) + E_m\right) \tag{2.2}$$

N is the total number of channels per platelet, γ the single channel conductance, P_o the channel open probability, and z the number of elementary charges per ion (2 in the case of calcium). The quantity N_A/F (Avogadro's number divided by the Faraday constant) represents the number of elementary charges per second per Ampere of current and is necessary to convert from units of current to moles of calcium per second. In this general equation, $[Ca^{2+}_{out}]$ represents the calcium concentration in the outer compartment and $[Ca^{2+}_{in}]$ represents calcium concentration in the inner compartment, e.g. for SOCs $[Ca^{2+}_{out}] = [Ca^{2+}]_{ex}$ and $[Ca^{2+}_{in}] = [Ca^{2+}]_{cyt}$. For purposes of determining SOC current, the product $N*P_o$ is equal to the total number of open SOC channels which is obtained from the MWC equations which will be discussed in Section 2.4.2.

Using the Hodgkin and Huxley framework, the plasma membrane is modeled as an RC circuit where fluxes of different ions are considered to be a set of resistors in parallel, we arrive at the following equation for modeling the change in membrane potential over time [111]:

$$\frac{dE_m}{dt} = \frac{1}{C_M} \times I_{Ca} \tag{2.3}$$

Calcium flow across the membrane, I_{Ca}, is the sum of all sources of current such as flow through pumps, channels, or passive leakage. The specific membrane capacitance, C_M, is a relatively conserved quantity across cell types [112] and for this study is estimated to be approximately 2 μF/cm^2 based on whole-cell patch clamp measurements that suggest platelet specific capacitance is somewhat higher than the 1 μF/cm^2 value typically seen in other cell types due to platelets' extensive surface invaginations [113]. Resting potential across the plasma membrane is maintained by voltage-dependent K^+ channels and has been estimated with voltage sensitive fluorescent dyes to be between -60 and -70 mV [6, 114, 115]. In practice in human platelets, plasma membrane potential (V_{PM}) is fairly constant during platelet activation by common agonists [115]. The resting potential across the DTS membrane (V_{IM}) is much less certain and remains unmeasured. The fact that slow calcium leakage from the endoplasmic reticulum is observed in the presence of SERCA inhibitors implies resting V_{IM} is more inside negative than the reversal potential of Ca^{2+} across the IM. Assuming a resting $[Ca^{2+}]_{dts}$ of 300 μM, V_{IM} must be greater than -100 mV [116]. Experiments in mouse pancreatic acinar cells [117] and rat sensory neurons [118] in which $[Ca^{2+}]_{cyt}$ was held constant with a BAPTA/Ca^{2+} buffer solution, calcium stores were depleted using SERCA inhibitors and store Ca^{2+} content measured with Mag-Fura2 found that stores plateau at a level greater than clamped $[Ca^{2+}]_{cyt}$. Assuming these plateaus are the result of net zero flux out of IM Ca^{2+} channels, from Eq. (2.2) one can calculate a V_{IM} as high as -74 mV.

2.4 SOCE Modeling

Several important features of SOCE have only recently been elucidated. SOCE activation consists of the calcium sensor STIM1 [65, 119] unbinding Ca^{2+} from its DTS-facing EF hand domain when $[Ca^{2+}]_{dts}$ drops relative to its K_d. Calcium unbinding allows STIM1 oligomerization, translocation to regions of the DTS membrane in close opposition to the plasma membrane, and finally association with tetrameric [120, 121] Orai1 protein channels in the PM. Orai1 passes current when at least one dimer is bound. We model the active form of STIM1 as a STIM1 dimer ($STIM_2$) and model the first two steps using mass action kinetics. STIM1 dimerization is assumed to be diffusion-limited. Patch clamp studies on larger mammalian cells indicate that store-operated current is inwardly rectifying, i.e. that the channels only allow current into the cell and do not operate in reverse under physiological conditions [122]. Platelets possess several other isoforms of STIM and Orai [99, 123]. Of these, STIM1 and Orai1 are the best studied and they are the most likely candidates for the components of functional SOC channels. For the purpose of this study, we refer to STIM1 and Orai1 as simply STIM and Orai.

2.4.1 Puncta formation

STIM and Orai are localized in separate membranes that require close contact for SOC activation [81, 124]. Store depletion causes STIM and Orai to undergo a rearrangement from being diffusely distributed in their respective membranes to a co-localized state at junctions between the IM and PM called puncta [65]. STIM can enter

the puncta by two mechanisms. One is passive diffusion (D ~ 0.1–0.15 $\mu m^2/s$) [69]. This mechanism accounts well for the time lag between STIM oligomerization and puncta formation in larger mammalian cells [125], however platelets are small enough that timescales for diffusion limited translocation would be < 1 s. When STIM puncta entry was modeled in this fashion (i.e. STIM in the puncta is essentially equal to total bulk STIM due to fast diffusion), we observed that the simulation could not satisfy homeostatic constraints on calcium while simultaneously observing significant contribution of SOCE to $[Ca^{2+}]_{cyt}$ following IP_3 stimulus. Thus, we modeled $STIM_2$ entry into the puncta with a $[Ca^{2+}]_{cyt}$-dependent Hill function applied to bulk IM $STIM_2$.

$$(STIM_2)_p = \theta_p \times STIM_2 \tag{2.4}$$

$$\theta_p = \alpha\left(\frac{[Ca^{2+}]_{cyt}^n}{K_M^n + [Ca^{2+}]_{cyt}^n}\right) + 0.01 \tag{2.5}$$

Only STIM dimers ($STIM_2$) are allowed to enter the puncta on the basis of evidence that STIM oligomerization precedes puncta formation [125]. Eq. (2.5) effectively reduces the amount of $STIM_2$ available for binding to Orai as only STIM in the puncta ($(STIM_2)_p$) is able to interact with Orai. The parameter α represents the maximum fraction of $STIM_2$ that can enter the puncta and was set to 0.2. K_M is the value of $[Ca^{2+}]_{cyt}$ at which θ_p is 50% of its maximum value; n is the Hill coefficient. The offset of 0.01 is needed to prevent θ_p being much less than unity at rest; $\theta_p << 1$ would lead to scenarios where $[Ca^{2+}]_{cyt}$ is the more dominant regulator of SOCE activity than $[Ca^{2+}]_{dts}$ which goes against the current understanding of the process. This regulation could represent an unidentified scaffold or helper protein that is regulated by $[Ca^{2+}]_{cyt}$ and necessary for

$STIM_2$ puncta entry. Alternatively it also could represent an increase in the amount of surface contact between the IM and PM as a result of actin-dependent cytoskeletal reorganization [126].

2.4.2 Channel Assembly

A recent study employing Orai tetramers fused with variable numbers of STIM dual C-terminal domains has shown a graded relationship between the number of $STIM_2$ bound and the activation state of the SOC channel [84]. To model association of $(STIM_2)_p$ with Orai, we adopt a similar Monod-Wyman-Changeux (MWC) [85, 127] equilibrium framework to model cooperative ligand binding. Channels exist in four states having 0 to 4 $STIM_2$ ligands bound. Each channel state can either be open (O, OS, OS_2, OS_3, OS_4) or closed (C, CS, CS_2, CS_3, CS_4). $(STIM_2)_p$ binds to Orai tetramers with negative cooperativity and channels open with positive cooperativity as a function of the number of $(STIM_2)_p$ bound. To satisfy mass balance all channel states (open and closed) must sum to the number of Orai tetramers. All states have the same conductance, but only open channels can pass current. At any given instant, not all $(STIM_2)_p$ is bound to Orai. The concentration of $(STIM_2)_p$ accessible to (i.e. in the puncta) but not bound to Orai is called S_f and is obtained by mass balance. Figure 2.2 *D* shows the possible transitions that can occur among these 10 states; the equations corresponding to these relationships are given in Table 1. General equations to represent the equilibrium relationships are

$$O = \frac{L}{C} \quad ; \quad i = 0$$
$$OS_i = OS_{i-1}\left(\frac{4-(i-1)}{i}\right) f a^i K_a S_f \quad ; \quad i = 1:4 \tag{2.6}$$

In these equations, L is the intrinsic opening equilibrium constant, K_a is the association constant for $(STIM_2)_p$ binding Orai, a is the binding cooperativity factor, and f is the

opening cooperativity factor [85]. Similar equations can be written for the closed states. The values for fixed parameters *f, a, K_a* and *L* were selected to yield an average open probability of ~0.8 at saturating levels of $STIM_2$ (see the Supporting Information of [85]) based on the results of noise analysis performed in store-depleted Jurkat T cells [63]. Following a procedure similar to that of Hoover et al., we generated analytic solutions to these 9 nonlinear equations coupled with mass balances on total $(STIM_2)_p$ and Orai using the MATLAB Symbolic Toolbox; these equations are listed in Appendix A. These algebraic equations are in terms of Orai and S_f. However at model runtime it is Orai and $(STIM_2)_p$ that are known from the kinetic equations discussed in previous sections. We used a linear set search algorithm to search for values of S_f which give the correct solutions for sets of pairs of Orai and $(STIM_2)_p$. The result was a two dimensional lookup table (LUT) that returns S_f as a function of Orai and $(STIM_2)_p$. Linear interpolation is used to calculate S_f at points not recorded in the LUT. Using a LUT in this way is much faster than having to search for the value of S_f that solves the equations given [Orai, $(STIM_2)_p$] at every time step of a simulation despite the significant extra memory overhead that is involved. With S_f in hand, the channel states can be calculated from the analytic solutions to the MWC equations. Figure 2.3 *A – E* illustrate the evolution of SOC states as a function of $(STIM_2)_p$ and Orai.

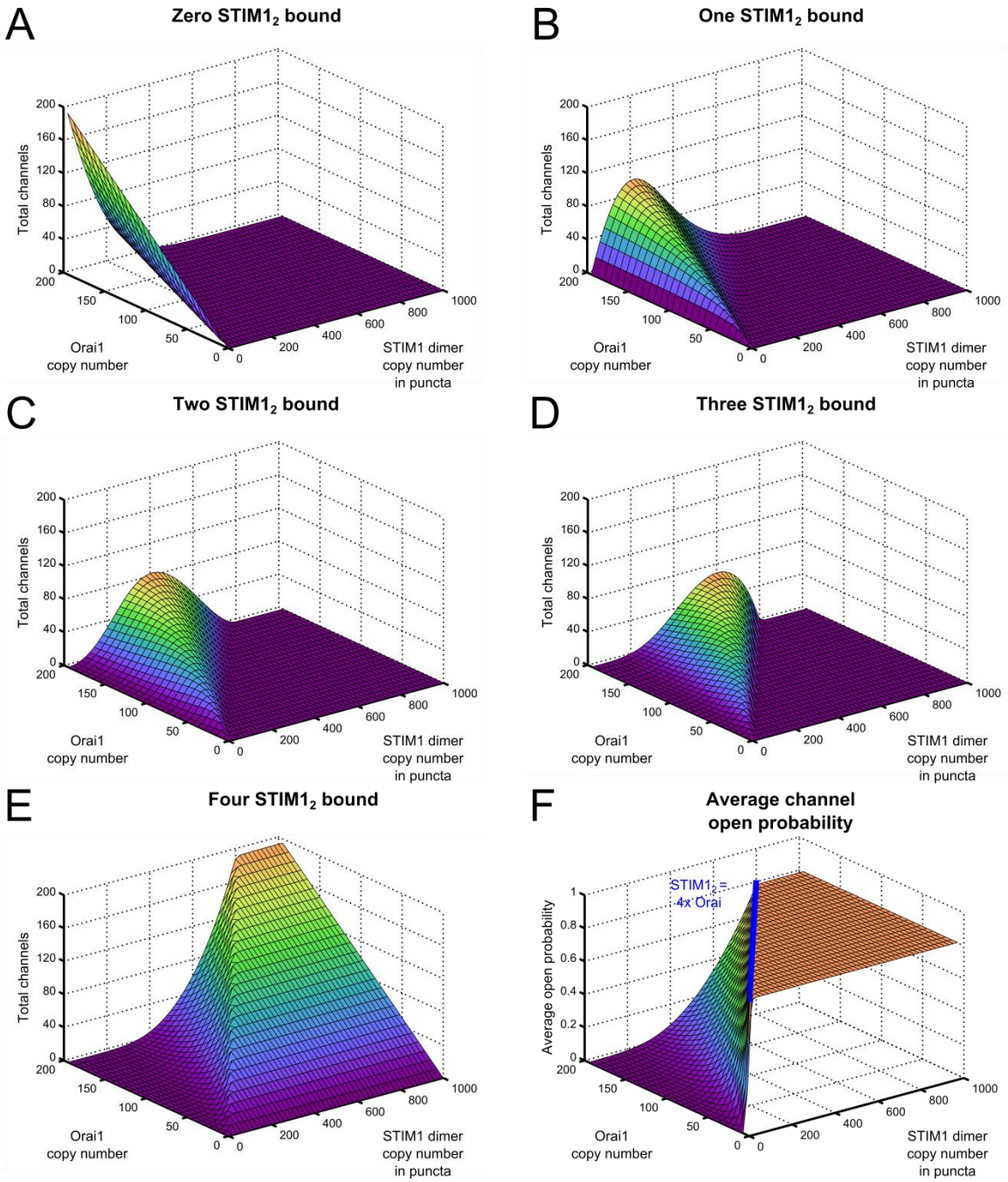

Figure 2.3 Analytical solutions to MWC equations as a function of interacting Orai and STIM dimers.

(*A* – *E*) These panels present the distribution of SOC states with 0 – 4 STIM ligands bound for variable numbers of Orai tetramers and STIM dimers. To determine these quantities, S_f is estimated at each [Orai, $(STIM_2)_p$] pair from the LUT and the channel states are calculated using the expressions in Appendix A. (F) P_{avg} as a function of Orai tetramers and STIM dimers. The line $[STIM1_2] = 4 \cdot [Orai]$ in the STIM-Orai plane is

overlaid in blue. When $STIM_2$ is greater than 4 times the number of Orai tetramers, all SOCs exist with four $STIM_2$ ligands bound and P_{avg} becomes equal to P_{o4}.

The open probability of channel state *i* is the ratio of the open channels in state *i* divided by the total number of channels in state *i*

$$P_{oi} = \frac{OS_i}{CS_i + OS_i} = \frac{Lf^i/K_a^i}{1 + Lf^i/K_a^i} \tag{2.7}$$

and is a fixed quantity for each channel state. The second equality in Eq. (2.7) comes from substituting in the appropriate expressions for OS_i and CS_i which are given in Appendix A. Table A.1 lists these values.

SOC channel state P_o	Value
P_{o0}	0.00001
P_{o1}	0.00142
P_{o2}	0.0198
P_{o3}	0.223
P_{o4}	0.803

Table 2.2 Individual SOC channel state open probabilities.

Presented are the open probabilities of the tetrameric Orai channels with zero to four STIM dimer ligands bounds. P_o values are calculated according to Eq. (2.7). In the model P_{o0} is rounded to zero.

Average open probability (P_{avg}) is the sum of all open channel states divided by the total number of channels (i.e. the number of Orai tetramers) and is shown in Figure 2.3 *F*. When $(STIM_2)_p = 0$, P_{avg} is zero as all channels have zero $(STIM_2)_p$ bound. As the amount of $(STIM_2)_p$ exceeds Orai by four fold (indicated by the blue line), all channels exist with four $STIM_2$ ligands bound and $P_{avg} = P_{o4} \sim 0.8$.

For purposes of modeling net current, or calcium flux, through SOCs we need only know the total number of open channels. Figure 2.4 *A* illustrates the relationship between the total number open channels and $(STIM_2)_p$ and Orai. The total number of open channels, that is

$$\sum_{i=1}^{4} OS_i$$

is equivalent to the quantity $N \cdot P_0$ in Eq. (2.3). Figure 2.4 *B* illustrates the general procedure for SOCE current (I_{SOC}) calculation. Because SOC current is inwardly rectifying [62, 122], in our model we do not allow SOCE to pass current in the reverse direction (i.e. out of the cell, which otherwise could occur in simulations run without Ca_{ex}).

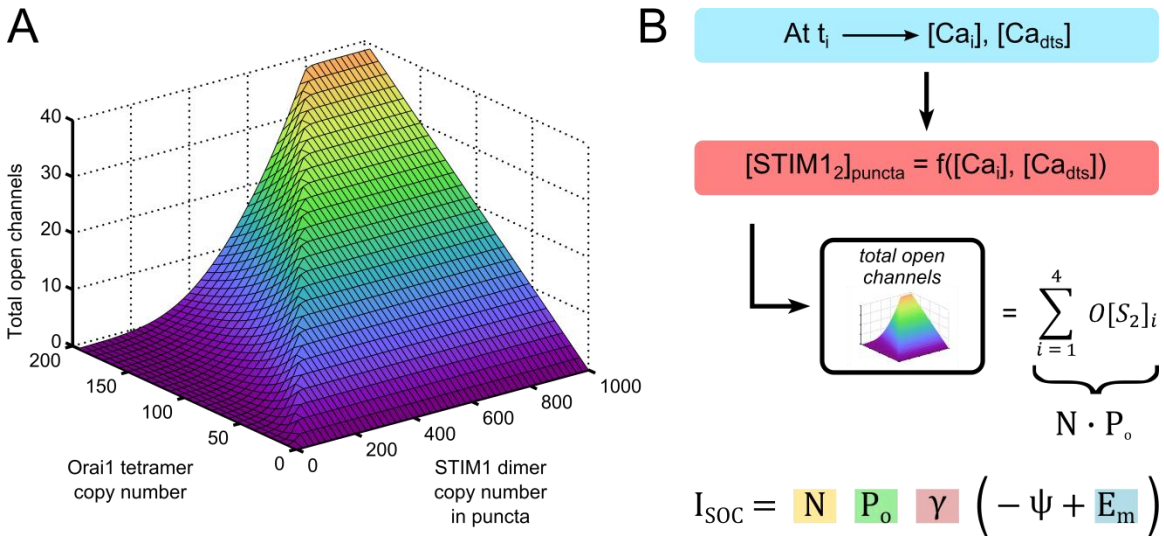

Figure 2.4 SOCE current determination.

(*A*) The total number of open SOCs is determined by the MWC equations as a function of $STIM_2$ in the puncta and Orai. (*B*) Procedure for determination of SOCE current. At every given time step in a simulation, the amount of $STIM_2$ in the puncta is determined by kinetic rate laws and Eq. (2.4). These quantities are passed to a pre-generated lookup table, presented as a surface in panel *A*, which yields the total number of open channels used in the equation for store-operated current.

2.5 IP_3 forcing function

Common platelet activation signaling pathways lead to PLC_β mediated hydrolysis of PIP_2 to produce IP_3, the IP_3R channel mediator. Agonist stimulated generation of IP_3 is well studied [128, 129]; previous work has modeled ADP mediated Ca^{2+} release via the G protein-coupled receptor $P2Y_1$ [57]. For the present study in which we explore combined IP_3-mediated and SOCE regulation of intracellular calcium, we removed upstream pathways leading to IP_3 generation in order to simplify the modeling process and reduce the number of unknowns requiring estimation. Thus instead of $[IP_3]$ dynamics being governed by a reaction network, we impose an explicitly defined supply of $[IP_3]$ as

a forcing function over time in order to simulate an activated platelet. To model [IP_3] over time we fitted experimental human platelet [IP_3] time course data [130] using a cubic Hermite interpolant [131]; this is a type of spline fit designed to minimize oscillations between data points. In the fitting data, values were only recorded to 30s post-stimulation. Platelet calcium dynamics typically occur over timescales longer than 1 minute; therefore time points greater than 30 s were extrapolated. Prior to fitting, the data was normalized by the resting value at t = 0 s. The general shape of the [IP_3] versus time curve, particularly in the region based on extrapolated data points, was loosely based on the results of previous modeling work [57]. In the final fit, IP_3 rises to about 5 fold higher than its resting value within 5 s of stimulation, and returns to a new steady level within 200 s. Other [IP_3] measurements in human platelets stimulated with a high dose of thrombin [132] also present a similar fold increase in [IP_3], indicating that a 5 – 6 fold increase may represent a saturating limit of the phosphoinositide pathway. Figure 2.5 illustrates the forcing function; this function was used for the parameter scans discussed in Chapter 3.

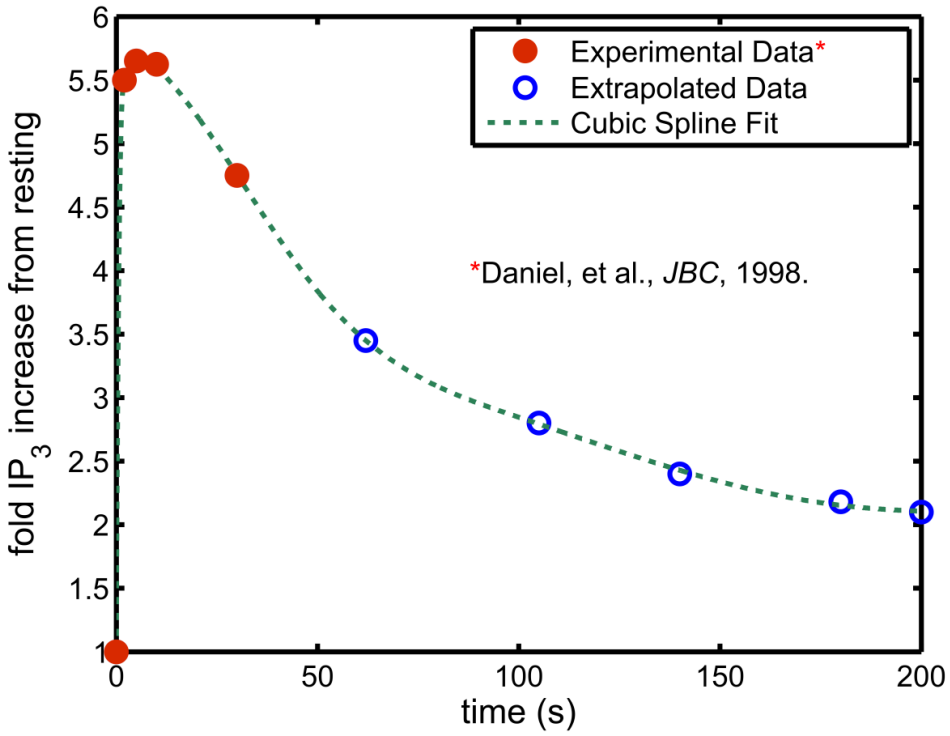

Figure 2.5 Spline fit IP_3 forcing function.

Normalized [IP_3] versus time data recorded in human platelet preparations stimulated with ADP at t = 0s were fitted with a cubic Hermite interpolating polynomial. Data points for fitting at t > 30s were estimated based on previous modeling of ADP mediated IP_3 generation.

For the IP_3 dose response simulations discussed in Chapter 3 in which it was desirable to have more precise control over the shape of the curve we cast [IP_3] as an exponential function of time. For an IP_3 dose delivered at t = 0 s, this equation is

$$[IP_3] = [IP_3]_0 \cdot \left[a t^{0.6} e^{(-bt)} + \frac{ct}{t+1} + 1 \right] \tag{2.8}$$

This equation is able to generate curves with shapes similar to the fit in Figure 2.5. The expressions in this equation and values for the fixed parameters *a*, *b*, and *c* as well as the exponent of 0.6 were determined through trial and error. The second rational function

term is present to allow $[IP_3]$ to settle to a value higher than baseline at long times. For both types of fits, the initial level of IP_3 ($[IP_3]_0$) varies with the model resting state.

Chapter 3

Steady-state kinetic modeling of regulators of calcium homeostasis

Computational models are useful for quantifying large reaction networks in complex biological systems [36, 58, 133, 134] which often exhibit very nonlinear behavior which makes them difficult to solve analytically or to predict using intuition. While data on reaction mechanisms, rate constants, and other physical parameters are frequently available in databases or scientific publications [135-137] (also see Table 2.1), integrating individually studied mechanisms to gain a systems level understanding of a model can be quite challenging. This is partly because such mechanisms are often studied *ex vivo* or in isolation. For example, the kinetic properties of SERCA have been assessed by isolating vesicles from COS-1 or HEK-293 cells engineered to express human SERCA 2 and 3 isoforms [103, 138]. One can imagine how the effective kinetic properties of such a complex protein may be different when observed in an environment outside the normal cellular milieu.

Thus one of the challenges of systems biology is tuning often large sets of parameters to get a model of integrated biological mechanisms to behave in a way which

is consistent with available experimental data; only after a model is so calibrated can it be expected to make realistic quantitative and qualitative predictions[4] [139]. In this context, "parameters" can also include diffusible species concentrations or protein copy numbers (i.e. elements of a model's initial condition vector). An additional hurdle is datasets themselves are often noisy or incomplete.

Numerous parameter estimation algorithms have been developed. These can fall into the category of being local or global. Local methods such as Nelder-Mead Simplex or Levenberg Marquardt [140] are less computationally demanding but are inappropriate for systems with complex objective function landscapes as they will (relatively) quickly converge to a local minimum [45, 141]. Methods can also be classified as deterministic or stochastic. Stochastic methods which randomly sample initial condition/parameter spaces for starting points are much less computationally demanding than deterministic methods but are also not guaranteed to reach a global minimum; such an uncertainty can usually be minimized for most problems when one allows for a reasonable number of samplings of state space. Some examples of stochastic global algorithms include particle swarm, simulated annealing, and genetic algorithms [45].

The behavior of complex, interconnected reaction networks is often more sensitive to models' initial conditions rather than to topology or fixed parameters [142]. Species concentrations may be expected to be more variable in nature as well. While rate constants are largely fixed by genetics and should be constant across healthy populations (genetic mutations are a notable and clinically relevant exception to this), stochastic

[4] This ignores the commonly encountered problem of overfitting, where a model has been optimized to fit a set of data very well but is not robust to state changes or is unable to predict the results of other related experiments.

variations at the molecular level in processes like transcription and translation can result in individual cells of the same type with different distributions of molecular constituents. As cell division results in some memory in the daughter cells as to the molecular makeup of the parent cell, these stochastic variations can manifest at the organismal level. We can use the platelet as a specific example. Platelets are formed by "blebbing" off from larger megakaryocytes in the bone marrow [143]. During this process, it is reasonable to imagine individual platelets acquiring different copy numbers of proteins and other biological molecules. Recent modeling work has suggested that the stronger response of platelets to thrombin versus the weaker agonist ADP can largely be explained by differences in copy numbers of their respective receptors [57], as the intermediate signaling steps leading to calcium mobilization are otherwise very similar for these two agonists. Thus the parameter scanning procedure discussed in the following sections primarily seeks to explore the effect of varying species concentrations and protein copy numbers on model's behavior.

3.1 Introduction: Platelet Calcium Balance

At rest, the platelet maintains stable sub-micromolar levels (40 – 100 nM) [6] of cytoplasmic calcium in balance with: nanomolar levels of IP_3 [132, 144, 145], high sub-millimolar storage pool calcium levels (100 to 400 μM) [146], and millimolar extracellular calcium (~ 1.5 mM) [147]. In achieving calcium homeostasis, the cell must balance the four interacting molecular modules: IP_3R, SERCA, PMCA, and SOCE. Additionally, at the moment of GPCR activation, the dynamics of IP_3 synthesis and

conversion mediate a large increase in intracellular calcium that is typically partially restored to resting levels while the calcium store refills following store operated calcium entry.

Several constraints must be simultaneously met by a dynamic model of calcium regulation. The model must:

1) Maintain low cytoplasmic calcium at rest in the presence of finite IP_3 levels.
2) Maintain high store concentration at rest, even in the absence of extracellular Ca^{2+}.
3) Present an increase in cytoplasmic calcium following stimulation.
4) Refill the store following transient cellular activation.

To meet these requirements in the resting cell the system is in a state of *dynamic equilibrium*; PMCA pumping out of the cell must equal SOCE flux into the cell. Also at rest, IP_3R flux must equal SERCA pumping. Importantly, placement of EDTA (calcium chelators) outside a cell must not cause a rapid depletion of store calcium. For example, platelets sitting in EDTA for an hour can still mobilize calcium following agonist stimulation. For platelets, resting cytosolic calcium is ~25 to 100 nM [7, 101] and DTS calcium is ~250 μM [146]. At resting $[Ca^{2+}]_{cyt}$, SERCA likely cannot pump against concentrations higher than 500 μM Ca which places an upper limit on store Ca^{2+} levels [148]. In the following two sections we present and apply a numerical method to investigate which sets of initial conditions allow the platelet calcium model to satisfy the above four homeostatic and dynamic constraints.

3.2 Monte Carlo method for exploring topologically enforced homeostatic constraints

Common stochastic parameter estimation routines are very abstract in that they view the problem as a black box by minimizing an objective function quantifying the difference between model output (or multiple outputs) and set(s) of data. The method used here is different in that it exploits the system's programmed physiology to search for resting configurations which are candidates for viable models. This method has the advantage of being completely independent of experimental time course data.

Where data on the cell's resting state is unavailable, intuition can be used to estimate a feasible sampling range. For example, a cell can reasonably be expected to have at least one copy of a protein. Similarly, a cell can only fit so many molecules inside itself. For example, assuming a spherical platelet of 3 μm diameter and an average transmembrane protein cross-sectional size of 35 nm^2, fewer than 200,000 proteins could fit into the plasma membrane. These arguments are simplistic and ignore the presence of other proteins (or even phospholipids in the case of our membrane example) in the system but are still useful as an order of magnitude estimate on the upper bounds for sampling ranges.

With a sampling space established, samples can be randomly drawn from this space and passed as initial conditions to the model and the model simulated until reaching steady state. Note that this parameter estimation scheme applies just as well to fixed parameters; these quantities can be considered to be state variables whose rate of change is zero. This scheme is summarized in Figure 3.1.

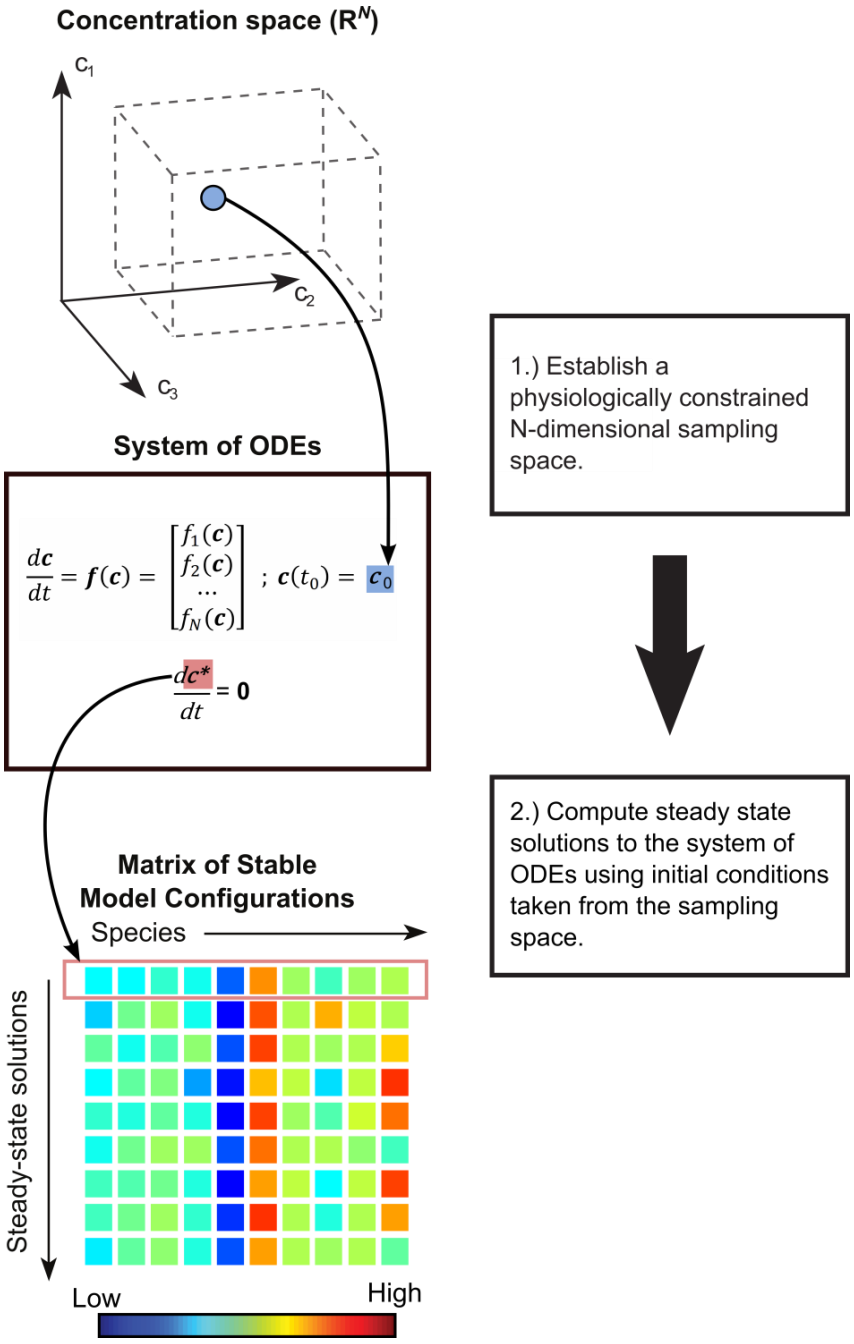

Figure 3.1 Monte Carlo state and parameter space scanning routine.

First one defines a physiologically derived sampling space with a number of dimensions equal to the number of unknowns in the system. Initial conditions (and parameters) can be drawn from this space, and the model is simulated to steady state. This gives the modeler a set of resting configurations which can then be further analyzed or filtered based on static or dynamic criteria.

To apply this method to our model, we densely sampled a 12-dimensional space of several protein species (IP_3R, SERCA, STIM, Orai, CaM, and PMCA), non-protein species ($[Ca^{2+}]_{cyt}$, $[Ca^{2+}]_{dts}$, $[IP_3]$), V_{IM}, and two unknown fixed parameters (K_m, n) in the model (see Table 3.1). For proteins, the search space was in a local region constrained by available LCMS data [116]. In general, copy numbers were allowed to vary by a factor of 2 above and below the measured values. All other rate parameters were fixed. V_{PM} was set to -60 mV [114] and $[Ca^{2+}]_{ex}$ to 1.2 mM. Resting states were accepted based on $[Ca^{2+}]_{cyt}$, $[Ca^{2+}]_{dts}$ and $[IP_3]$ satisfying the physiologic constraints outlined in the column "Acceptance Criteria" in Table 3.1 and discussed in Section 3.1. There is no need for acceptance criteria to be placed on the total protein counts as there is no protein generation or degradation present in the model.

State/Param (units)	Known Values	Sampling Range	Acceptance Criteria	Reference
Ca_{cyt} (nM)	75	10 – 100	25 – 100	Siess, 1989, [7]
Ca_{dts} (μM)	250	80 – 1000	100 – 400	Sage, 2011, [146]
IP_3 (nM)	~ 130	20 – 200	≥ 1	Nakagawa, 2002, [145]
IP_3R (copies/cell)	1,700	850 – 3,400		Burkhart, 2012, [99]
SERCA (copies/cell)	16,300	4,600 – 18,400		Burkhart, 2012, [99]
STIM (copies/cell)	3,700	1,850 – 7,400		Burkhart, 2012, [99]
Orai (copies/cell)	425	212 – 850		Burkhart, 2012, [99]
CaM (copies/cell)	15,600	7,200 – 32,500		Burkhart, 2012, [99]
PMCA (copies/cell)	640	320 – 1,280		Burkhart, 2012, [99]
V_{IM} (mV)	> -100 mV	-100 – -60		Burdakov, 2005, [116]
K_M (nM)		100 – 300		This study
n		1 – 3		This study

Table 3.1 List of 12-dimensional state space sampling ranges.

The sampling space is chiefly derived from literature measurements. The units listed in parentheses in the first column also apply to values in the following three columns. Protein copy numbers ranges were generally set with upper and lower bounds 2-fold above and below mean values measured by LCMS. The acceptance criteria for $[Ca^{2+}]_{cyt}$ and $[Ca^{2+}]_{dts}$ are unequal to the sampling ranges because these species quickly get bound to proteins like SERCA or STIM1 or transported to other compartments after the model is initialized with a random initial condition vector making their final resting values oftentimes very different from their initial values; the sampling ranges were adjusted based on these facts to make it easier to find resting configurations satisfying the acceptance criteria. The acceptance criterion for IP_3 exists to ensure the number of IP_3 copies is greater than unity.

We accepted a sample as being at steady state if the relative absolute value of the ∞-norm of the rate of change vector was less than 0.1%. Expressed mathematically:

$$\left| \frac{\| d\boldsymbol{c}/dt \|_\infty}{\boldsymbol{c}} \right| < 0.001 \tag{3.1}$$

We did not consider configurations which exhibit oscillations; the number of such configurations which demonstrated oscillatory behavior was quite few (< 0.1% of steady states sampled).

3.3 Results

3.3.1 Filtering configurations based on robustness and dynamic constraints.

A dense sampling of over 2.6 million initial conditions from this 12-dimensional sampling space produced 150,000 steady states which satisfied the homeostatic requirements that were enforced. An important additional resting criterion is that states remain stable upon Ca_{ex} removal; this is particularly important in the context of our modeling as Ca_{ex} chelation is an important experimental technique for measuring the contribution of extracellular calcium entry (e.g. SOCE) to the overall Ca^{2+} response. To apply this condition we selected for states that exhibited less than a 5 μM decline in $[Ca^{2+}]_{dts}$ over 333 s following Ca_{ex} removal. This constraint is supported by experiments in which cells did not respond to calcium re-addition after having been stored in EDTA for more than 10 minutes (implying their stores were not significantly drained) [149].

The set of accepted resting states were further characterized and grouped based on their responses to a 5.5-fold IP_3 stimulus (see Section 2.5 of Chapter 2). First, configurations were filtered for those that were responsive to IP_3 based on peak $[Ca^{2+}]_{cyt}$ reaching a concentration greater than 200 nM following IP_3 application. Second, configurations were filtered for those that also showed SOCE activity. This criterion was

based on difference in peak $[Ca^{2+}]_{cyt}$ in simulations with and without Ca_{ex} reaching a value greater than 100 nM. We chose to use $[Ca^{2+}]_{cyt}$ as the metric for SOCE activity as this quantity is commonly measured and numerous data in the literature point to a substantial difference in $[Ca^{2+}]_{cyt}$ in human platelets labeled with fluorescent dyes following agonist stimulation with and without Ca_{ex} present [126, 150, 151]; the value of 100 nM was based on the measurements of one study in particular which used ADP [150], a weaker platelet agonist. These filtering criteria and the number of resting states which satisfy each are tabulated in Table 3.2. In the analysis and discussion to follow these filters are applied sequentially such that configurations falling into the last group listed in Table 3.2 also satisfy all the other conditions. Notably, less than 0.06% of all sampled initial conditions satisfied all 4 homeostatic and dynamic constraints which indicates the system is well constrained by these criteria.

Condition	Mathematical constraint	States	Percent
Steady State Calcium	25 nM ≤ Ca_{cyt} ≤ 100 nM, 100 μM ≤ Ca_{dts} ≤ 400 μM	150,000	5.64%
Stable in EDTA	Resting DTS leak < 0.015 μM/s	18,932	0.71%
Active	Max(Ca_{cyt}) > 200 nM with IP_3	8,093	0.30%
SOCE	Δ(Max(Ca_{cyt}) in +/-EDTA) > 100 nM	1,513	0.06%

Table 3.2 List of resting configuration filtering constraints.

Resting configurations were divided into groups based on: (1) resting $[Ca^{2+}]_{cyt}$ and $[Ca^{2+}]_{dts}$ being within physiologic ranges; (2) calcium levels being stable upon Ca_{ex} removal; (3) active states in which $[Ca^{2+}]_{cyt}$ rises above 200 nM following 5.5-fold IP_3 stimulus; (4) difference in $[Ca^{2+}]_{cyt}$ following 5.5-fold IP_3 stimulus with and without Ca_{ex} is at least 100 nM. Constraints are applied sequentially, e.g. resting configurations satisfying the SOCE constraint also satisfy those constraints listed in the rows above. Percentages are relative to the initial set of 2.6 million resting configurations.

Figure 3.2 presents the probability distributions of each search dimension for the three filtered populations (i.e., functional phenotypes) of resting initial condition configurations. The filter is indicated by the shaded circle and corresponds to the descriptions in Table 3.2. Where applicable, an arrowhead indicates measured resting values. The model topology and parameterization and filtering criteria placed sufficient constraint to push resting $[Ca^{2+}]_{cyt}$, $[Ca^{2+}]_{dts}$ to the lower end of the search range. Platelets that met all criteria had IP_3 levels constrained fairly narrowly between 20 and 40 nM (< 200 copies per platelet), somewhat lower than the measured 130 nM value [145]. The model accepts lower $[Ca^{2+}]_{dts}$ than the measured value of ~250 μM [146]. This is likely due to the constraints our sampling ranges have placed on the ratio of SERCA to IP_3R.

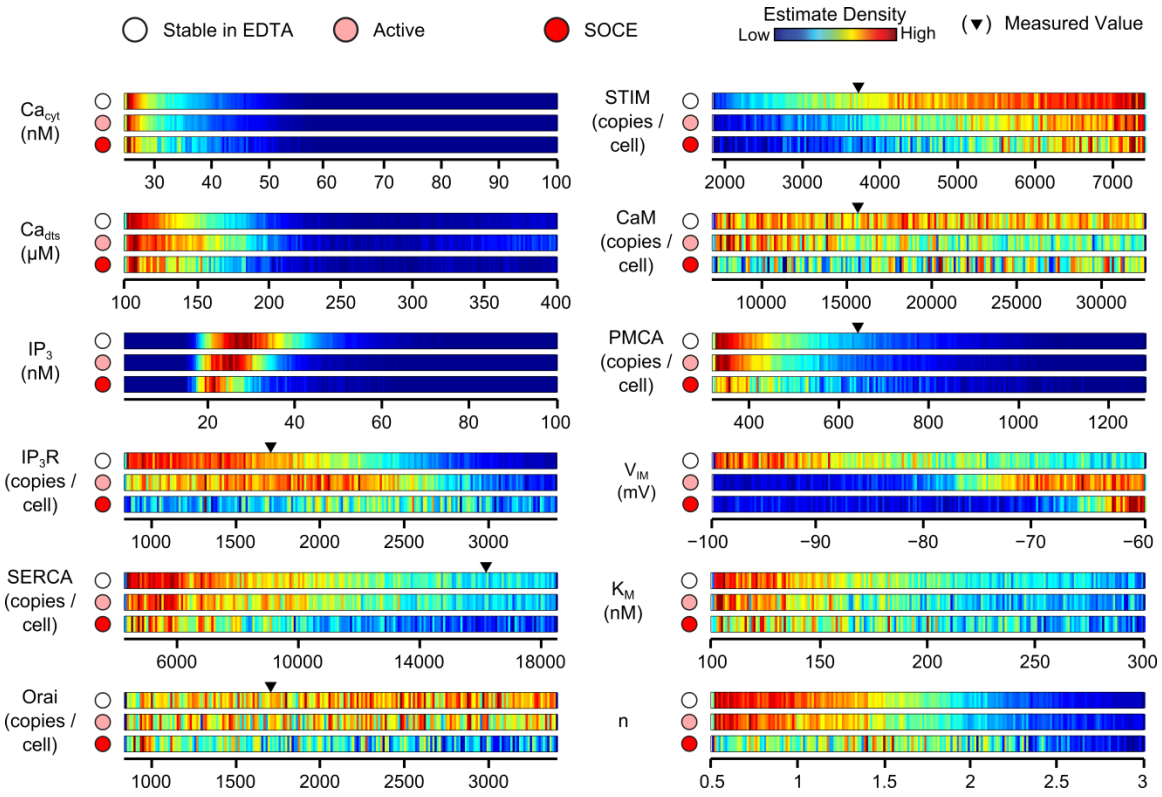

Figure 3.2 Resting configuration probability distributions.

Probability distributions of model species and parameter configurations satisfying the "Stable in EDTA", "Active" and "SOCE" filtering constraints. All distributions also satisfy the "Steady State Calcium" criterion. An arrow at the top of the first bar for protein species indicates the experimentally measured protein copy numbers [99].

Currently, no experimental measurements of V_{IM} exist due to technical difficulties in measuring potential across the ER membrane using patch-clamp. We allowed our scans to sample V_{IM} in the range of -100 to -60 mV based on arguments in the Section 2.3. Model configurations stable in EDTA show a lower (i.e., more negative) inner membrane potential however, in stark contrast, configurations that are responsive to IP_3 as well as those which also demonstrate SOCE posses a higher V_{IM} that clusters near the upper bound of the sampling range. The parameters *n* and K_M which govern STIM entry into

puncta appear to become more monodisperse as additional filtering conditions are applied.

3.3.2 Transient behavior following IP_3 stimulus

Calcium release from the stores requires transient stimulation of IP_3R by IP_3. Literature measurements of IP_3 time courses in human platelets stimulated by strong doses of agonists such as thrombin and ADP show $[IP_3]$ rising sharply by several fold and peaking within 2.5 – 30 s following agonist delivery [132, 144, 145]. Furthermore, $[IP_3]$ and $[Ca^{2+}]_{cyt}$ return to nearly resting levels 30 – 60 s following agonist stimulation [130] as IP_3 is degraded by phosphatases and Ca^{2+} is pumped back into the DTS. Figure 3.3 shows the response of a subset of the fully filtered population of resting states to an IP_3 stimulus constructed to mimic these measured behaviors (see Section 2.5).

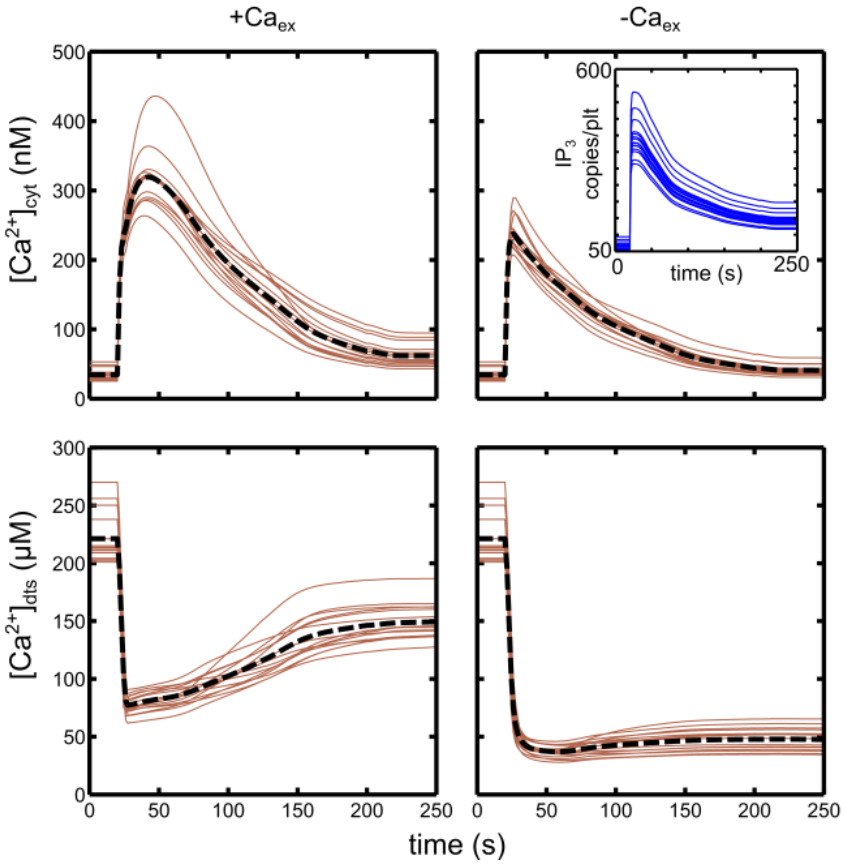

Figure 3.3 Representative model responses to IP_3 stimulus.

15 resting states satisfying all filtering criteria were stimulated with 5.5 fold IP_3 dose starting at t = 20 s. The IP_3 doses are illustrated in the inset in the upper right panel. (*B*) Calcium traces for DTS and cytosolic Ca^{2+} of a representative configuration taken from this population to the six IP_3 doses shown in the inset in the upper right panel. The colors of the curves correspond to the IP_3 dose. Left column: $[Ca^{2+}]_{ex}$ = 1.2 mM; right column: $[Ca^{2+}]_{ex}$ = 1 pM.

$[Ca^{2+}]_{cyt}$ generally peaks within 15 – 20 s of IP_3 application (the $[IP_3]$ time courses which are shown in the inset peak ~3 s following application), and reaches a higher peak and remains more sustained in the presence of extracellular calcium. $[Ca^{2+}]_{dts}$ partially refills in simulations run with Ca_{ex} and shows no refilling in calcium-free media. $[Ca^{2+}]_{cyt}$ peaks earlier in simulations without Ca_{ex}; this is due to SOCE continuing to be partially active

as stores refill rather than there being a time delay in I_{SOC} activation following store depletion (see Figure 3.6 *A*).

Figure 3.4 *B* shows the calcium responses of a representative configuration from the stable population to a series of increasing [IP_3] stimulations shown in Figure 3.4 *A*. The 1.5x and 2x stimulations were too weak to elicit substantial SOCE; at higher IP_3 doses, stores become depleted enough that SOCE manifests itself via elevated $[Ca^{2+}]_{cyt}$ and substantial store refilling. The model predicts faster time to peak $[Ca^{2+}]_{cyt}$ at stronger IP_3 doses in $–Ca_{ex}$ simulations; in contrast, in $+Ca_{ex}$ simulations peak $[Ca^{2+}]_{cyt}$ is higher and delayed until stores refill to sufficiently inactivate SOCE (also see Figure 3.6).

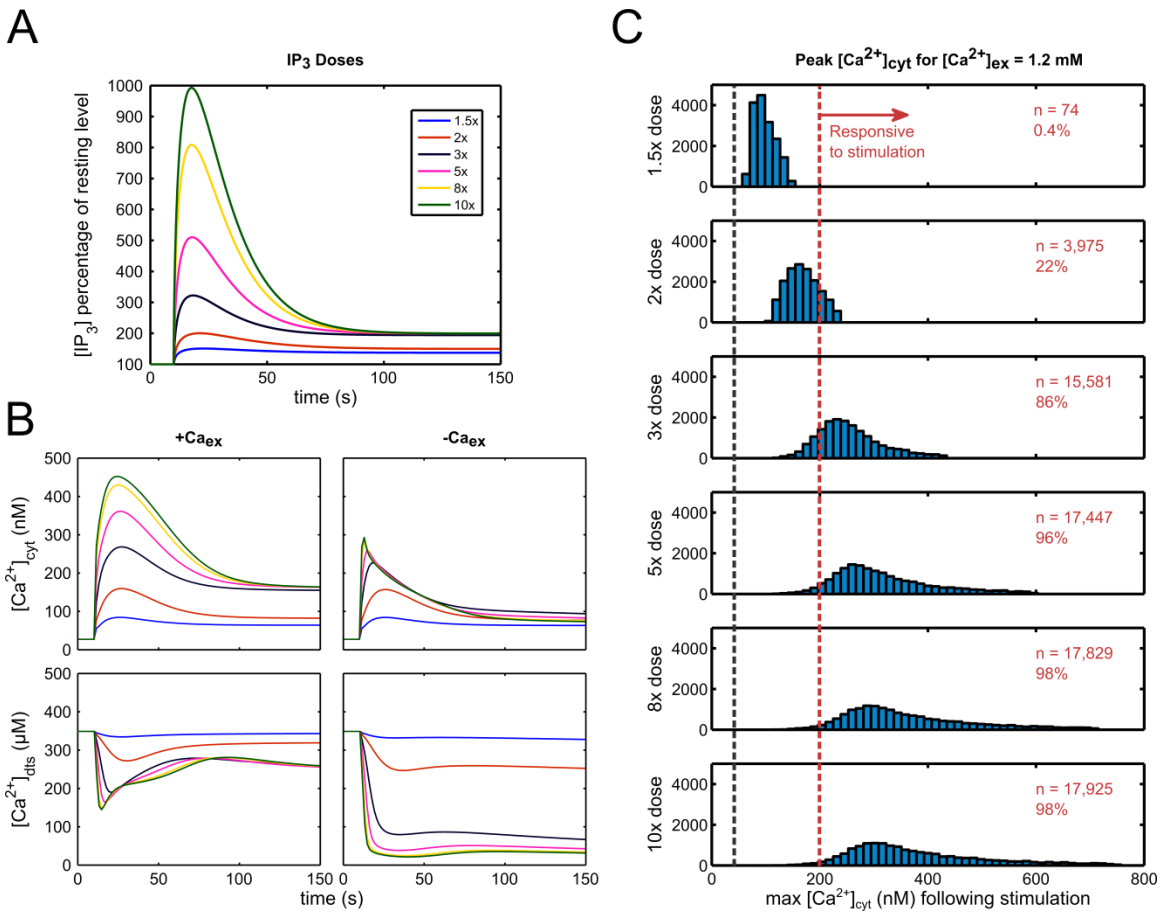

Figure 3.4 Response of population stable in EDTA to a dose of IP_3.

*(*A) The population of states satisfying the stability criterion (n = 18,932) were stimulated with a dose of IP_3 which is summarized as a percentage increase over baseline. The IP_3 stimulus begins at 10 s. (*B*) Calcium traces for DTS and cytosolic Ca^{2+} of a representative configuration taken from this population to the six IP_3 doses presented in panel A. The colors of the curves correspond to the IP_3 dose. Left column: $[Ca^{2+}]_{ex}$ = 1.2 mM; right column: $[Ca^{2+}]_{ex}$ = 1 pM. (*C*) Distributions of peak $[Ca^{2+}]_{cyt}$ for each IP_3 dose. The black vertical dotted line indicates mean resting $[Ca^{2+}]_{cyt}$ and the red dotted line indicates our cutoff for a configuration to be considered "responsive" to stimulus. The number and percentage of configurations satisfying this criterion are indicated in red in the upper right of each histogram. Increasing the IP_3 dose makes more states satisfy this criterion; in addition peak $[Ca^{2+}]_{cyt}$ largely saturates beyond 5x IP_3.

Figure 3.4 *C* shows histograms of peak $[Ca^{2+}]_{cyt}$ of the entire set of stable configurations (n = 18,932) following application of each dose of IP_3 in panel *A*. Stronger doses of IP_3 predictably result in higher average $[Ca^{2+}]_{cyt}$; this effect saturates past 5x IP_3.

Figure 3.5 compares the model's $[Ca^{2+}]_{cyt}$ response to the 10x IP_3 stimulation (left) with experimental time course data (right) from human PRP fluorescently labeled with fura-2 and treated with 40 μM ADP at t = 20s [150]. The simulations generally agree very well with the experimental data; there is a small time delay of ~20s in peak $[Ca^{2+}]_{cyt}$ in the $+Ca_{ex}$ simulation compared to experiment; this time delay is reproducible using other model initial conditions (data not shown).

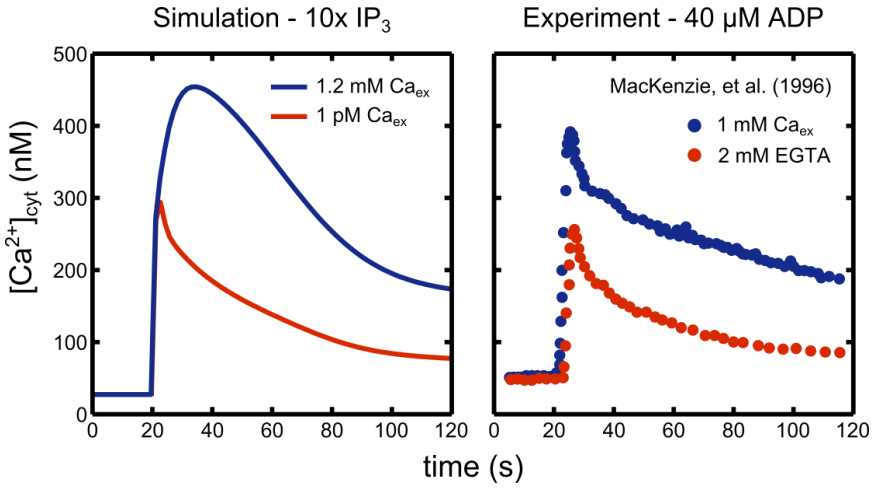

Figure 3.5 Comparison of model output with experimentally measured calcium transient.

The 10x IP_3 simulated $[Ca^{2+}]_{cyt}$ time course from Figure 3.3 *B* (left) is compared with calibrated fura-2 time course data in human platelets treated with 40 μM ADP at t = 20 s (right) [150].

To attempt to explain the source of this time delay, Figure 3.6 *A* plots simulations of Ca^{2+} flux via PMCA (blue curve) and SOCE (red curve) following a 5.5x IP_3 dose applied at t

= 10s. The corresponding $[Ca^{2+}]_{cyt}$ and $[Ca^{2+}]_{dts}$ traces are shown in Figure 3.6 *B* with peak $[Ca^{2+}]_{dts}$ and $[Ca^{2+}]_{cyt}$ times indicated by the bolded solid and dashed lines, respectively. SOCE flux peaks at the time $[Ca^{2+}]_{dts}$ reaches its minimum. This implies there is no delay in SOCE activation with respect to $[Ca^{2+}]_{dts}$. As stores do not refill immediately, there is a slow inactivation of SOCE current which continues to drive $[Ca^{2+}]_{cyt}$ higher even after the stores have finished emptying; $[Ca^{2+}]_{cyt}$ does not peak until the SOCE flux is nearly overtaken by the PMCA flux out of the cell.

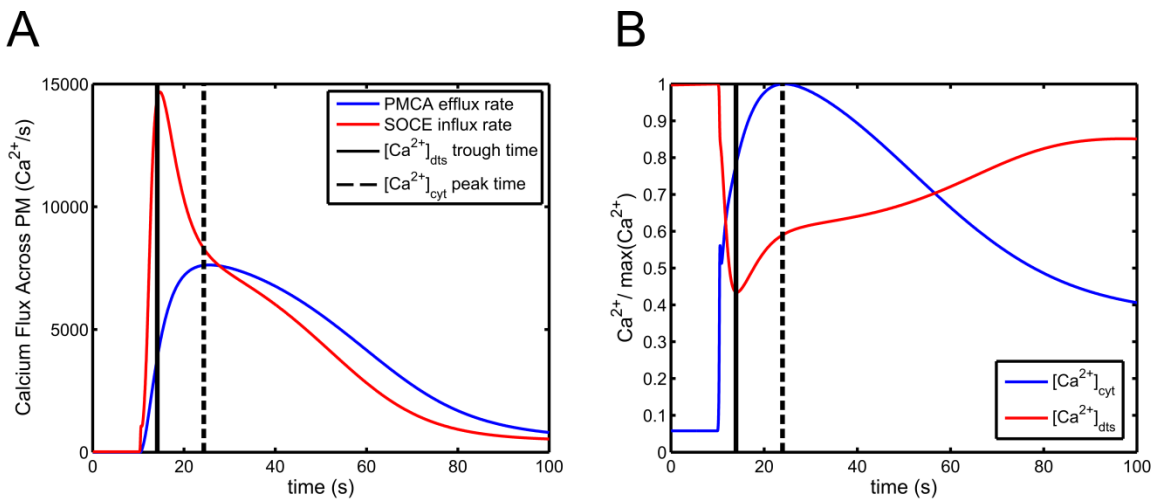

Figure 3.6 Time delay in +Ca_{ex} simulations is due to slow SOCE inactivation.

(*A*) This panel plots Ca^{2+} flux across the PM, the blue curve being Ca^{2+} flux out of the cell via PMCA, and the red curve Ca^{2+} flux into the cell via open SOCs. I_{SOC} peaks at about the time when $[Ca^{2+}]_{dts}$ reaches its minimum value (peak time indicated by a vertical solid black line). $[Ca^{2+}]_{cyt}$ does not peak (peak time indicated by a vertical dashed black line) until the extra Ca^{2+} influx into the cytosol is reduced to near zero by PMCA. (*B*) Calcium traces of $[Ca^{2+}]_{cyt}$ and $[Ca^{2+}]_{dts}$ corresponding to the simulation shown in *A*; each are normalized by their maximum value. The bolded vertical lines are the same as in panel *A*.

In Figure 3.7, model configurations in the stable in EDTA population were subjected to a 10x IP_3 dose at t = 0 s with $[Ca^{2+}]_{ex}$ set to 1.2 mM. Panel *A* shows no correlation between the time at which $[Ca^{2+}]_{cyt}$ reaches its peak and fractional store

refilling. Panel *B* shows that the peak $[Ca^{2+}]_{cyt}$ time decreases as the SERCA to IP_3R ratio increases. As SERCA and IP_3R act in direct opposition to one another, configurations with a higher SERCA / IP_3R ratio are able to refill stores more quickly.

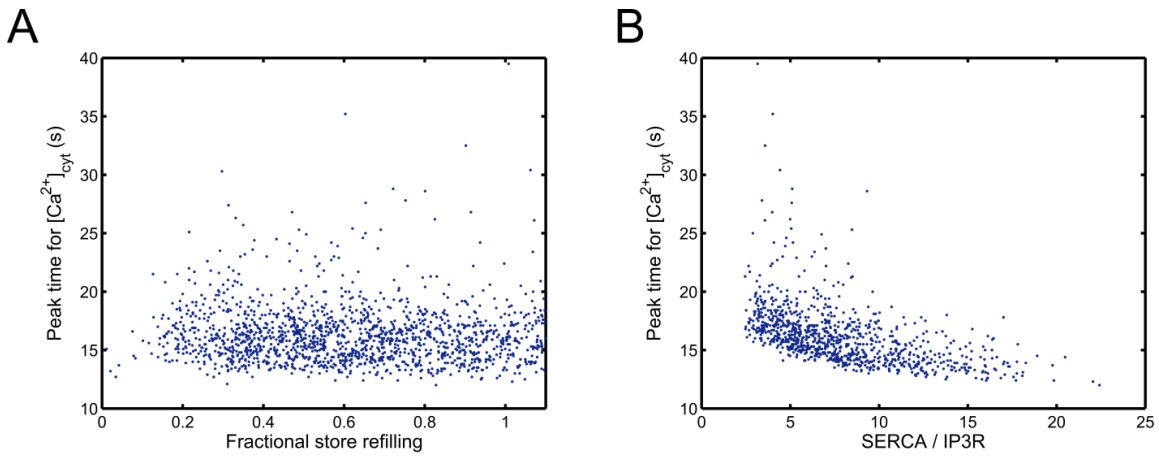

Figure 3.7 Rate of store refilling is an important determinant of peak $[Ca^{2+}]_{cyt}$ time in $+Ca_{ex}$ simulations.

(*A*) Scatter plot of the time at which $[Ca^{2+}]_{cyt}$ peaks versus fractional amount of store refilling reveals no correlation between the metrics. Fractional refilling is calculated as the final value of $[Ca^{2+}]_{dts}$ in a simulation divided by the initial drop following IP_3 stimulus. (*B*) Scatter plot of the time at which $[Ca^{2+}]_{cyt}$ peaks versus the SERCA / IP_3R ratio.

3.3.3 Perturbation of the fraction of STIM able to enter puncta

Next we explored the effect altering fixed parameters governing SOCE would have on the model's steady state and dynamics following stimulus. An *in silico* experiment like this is very much analogous to simulating the effect of a mutation in a gene. Genetic mutations can often have disastrous consequences for the organism. For example, mutations in the HEX A gene encoding the lysosomal protein hexosaminadase A result in a nonfunctional enzyme which is unable to remove an amino sugar residue

from GM_2 gangliosides, leading to a dangerous buildup of this compound in the brain [152]. These mutations are associated with Tay-Sachs disease.

For the work presented here, we focused on the parameter α which establishes the maximum fraction of $STIM_2$ that can enter the puncta (see Eqs. (2.4) and (2.5)). Mutation of the glutamate or aspartate residues responsible for Ca^{2+} binding in the STIM EF-hand domain leads to constitutive puncta entry and associated higher basal I_{SOC} [65, 86]. Following perturbation and after allowing for an adjustment phase of at least 200 s, the model was checked for being at steady state as per Eq. (3.1). The perturbations were performed on the resting configurations that satisfied all filtering conditions (n = 1,513; also see Section 3.3.1). α was perturbed from 0.2 (the initial value for all configurations) to 0.5, 0.75 and 1.

In Figure 3.8 we present resting $[Ca^{2+}]_{cyt}$ (left) and $[Ca^{2+}]_{dts}$ (right) distributions following parameter perturbation.

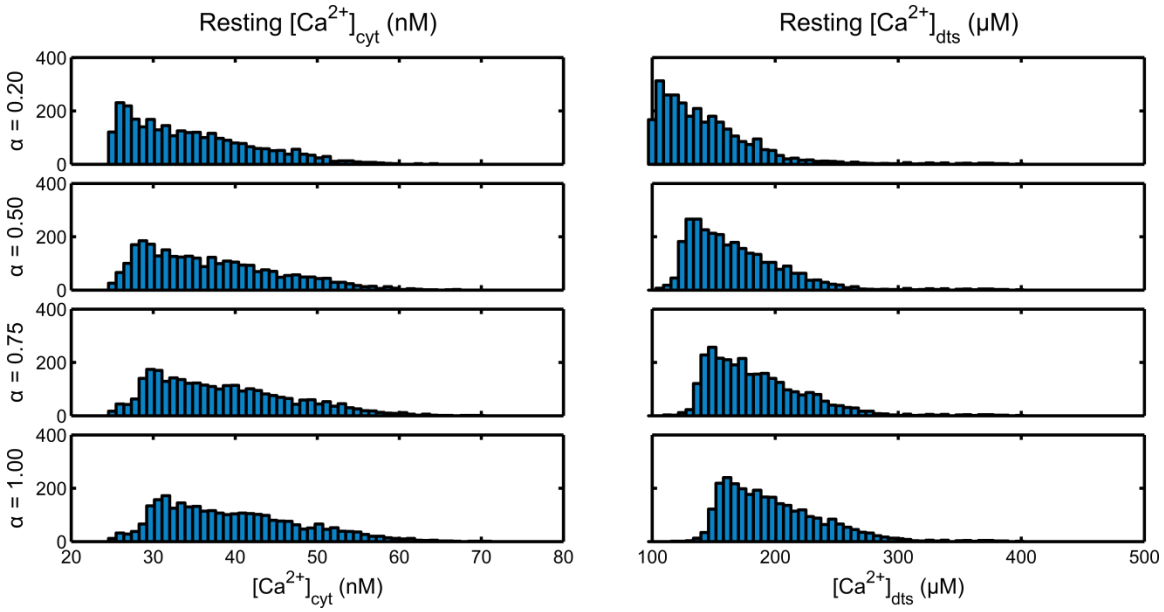

Figure 3.8 Resting Ca^{2+} for the state population satisfying all resting and dynamic constraints following α perturbation.

The fixed parameter α was altered to the levels indicated for the population of configurations that were stable in EDTA. The Ca^{2+} concentrations reported for α = 0.5, 0.75, 1 are those following adjustment to new steady state; α = 0.2 was the initial value used in all simulations in prior Sections.

$[Ca^{2+}]_{cyt}$ is very stable to all levels of perturbation. Raising α increases $[Ca^{2+}]_{dts}$ somewhat. Despite the relatively modest changes in models' resting states, peak $[Ca^{2+}]_{cyt}$ distributions resulting from a 5.5x IP_3 stimulus applied to the new resting states are right-shifted as α increases for simulations ran with 1.2 mM Ca_{ex} (Figure 3.9, left) but not without Ca_{ex} (Figure 3.9, right).

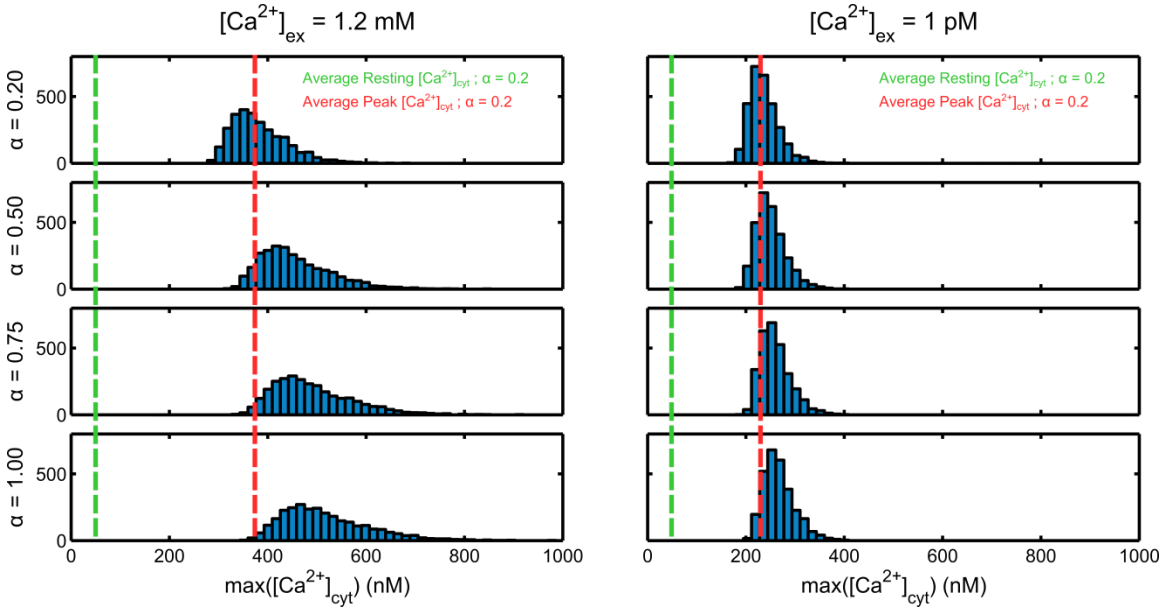

Figure 3.9 Peak $[Ca^{2+}]_{cyt}$ following IP_3 stimulus for the state population satisfying all resting and dynamic constraints following α perturbation.

A 5.5x IP3 stimulus was applied to the population of configurations stable in EDTA following adjustment of α to the indicated values. Simulations were run with Ca_{ex} set to 1.2 mM (left) or to 1 pM (right). The green and red dotted lines indicate average resting and peak $[Ca^{2+}]_{cyt}$ for α = 0.2.

These results imply the increase in peak $[Ca^{2+}]_{cyt}$ in $+Ca_{ex}$ simulations as α is raised is due to more $STIM_2$ entering the puncta following store depletion and not due to higher basal $[Ca^{2+}]_{dts}$ or high α being able to decouple SOCE from $[Ca^{2+}]_{dts}$ by strengthening the influence of $[Ca^{2+}]_{cyt}$ on the amount of $STIM_2$ available to Orai (see Eqs. (2.4) and (2.5)).

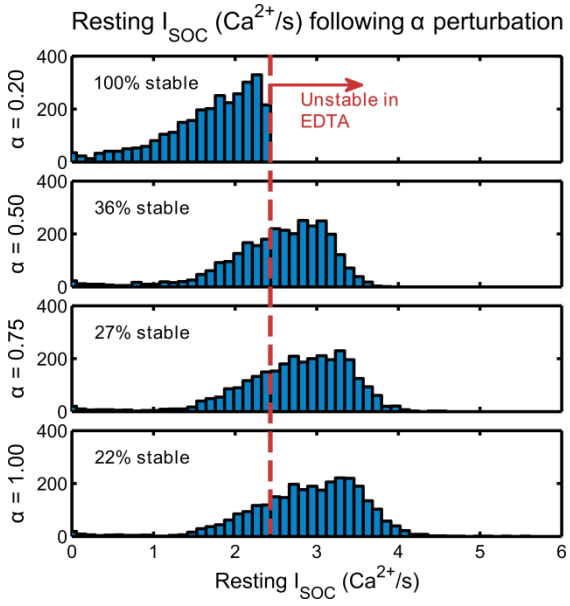

Figure 3.10 Increasing α leads to reduced system stability in Ca^{2+}-free media.

Histograms of resting I_{SOC} for the fully filtered state population following α perturbation to the indicated values. The red dotted line indicates the value of I_{SOC} above which the stability criterion (see "Stable in EDTA" in Table 3.2) would be violated.

In Figure 3.10 we observe the effect of α on resting I_{SOC}. Increasing the α parameter in the puncta formation equation reduces the number of stable configurations in the population initially satisfying all filtering conditions. A higher value of α increases the number of active $(STIM_2)_p$ at rest; resting I_{SOC} increases correspondingly due to there being more open channels. Configurations with higher resting I_{SOC} lose calcium more quickly following EDTA application. The I_{SOC} cutoff is equivalent to the rate of change of $[Ca^{2+}]_{dts}$ criterion indicated in Table 3.2; this is because PM flux is the rate-limiting step for Ca^{2+} leakage. As a more extreme example we could set the entire θ_p parameter to unity (i.e. making all $STIM_2$ is available to Orai) which causes the entire population of configurations that were previously viable according to our criteria to fail the stability in

EDTA criterion (data not shown). Thus a higher α is able to cause more STIM dimers to be present in the puncta under resting conditions, despite higher levels of store filling.

3.4 Discussion

This chapter has been devoted to solving the inverse problem discussed in the introduction as applied to a mechanistic model of SOCE in human platelets. In the context of this problem, the "fitting data" consisted of both homeostatic constraints derived from experiment and intuition and experimental $[Ca^{2+}]_{cyt}$ transients in human platelet populations stimulated in calcified and calcium-free conditions [150]. Our parameter scan results reveal how a model's topology and fixed parameters naturally enforce constraints on the steady state configurations that a model is able to exhibit. The model is able to take on physiologically acceptable configurations with mean values that differ by no more than a factor of two from experimentally measured values for protein copy numbers (typically measured with light scattering mass spectroscopy) or calcium concentrations. Low resting levels of IP_3 are required for system robustness and for appropriate dynamic response to physiologic agonists.

Multiple steady states (the 1,513 ICs meeting the filtering criteria, see Figure 3.2 and Table 3.2) are expected and were sought out because: (i) total protein measurements (Table 3.1) do not define the distribution of the protein sub-species (e.g. $SERCA_{E1}$, $SERCA_{E2}$, etc) within the individual modules (Figure 2.2) where the six measured protein levels for IP_3R, SERCA, STIM, Orai, CaM, and PMCA are actually distributed over 24 states/complexes (see Table 2.1) which are not known but must be consistent with the

topology, kinetic parameters, homeostasis requirement, and filtering criteria; (ii) cellular heterogeneity is expected around a population average measurement and variations for a particular protein could easily be ± 100 %; and (iii) the filtering criteria defined in Table 3.2 are based upon ranges and upper and lower bounds, not strict values (e.g. steady state $[Ca^{2+}]_{cyt}$ = 75 nM). The IC exploration range was also fairly restricted for IP_3R, SERCA, Orai, STIM, CaM, and PMCA around their measured values (Figure 3.2). The filtering criteria and model topology was more restrictive of allowed ICs for SERCA, STIM, and PMCA, but less so for IP_3R, Orai, and CaM suggesting less model sensitivity to the values of IP_3R, Orai, and CaM; these broader distributions are also partly a consequence of the relatively narrow sampling ranges used in comparison to prior work [57].

Membrane electric potential is an important parameter for modeling channel current as it affects the driving force for passage of charged particles across a membrane. The potential across the inner membrane (V_{IM}) is largely unexplored due to being difficult to assess with traditional patch-clamp techniques [116]. V_{IM} acts in opposition to the favorable calcium concentration gradient across the IM, effectively acting as a brake on calcium release and functionally placing a lower bound on $[Ca^{2+}]_{dts}$ by setting the Nernst potential at which calcium flux out of the DTS via IP_3R is zero (see Eq. (2.2)). In agreement with this idea, in our model resting configurations satisfying only the static constraint of being stable in EDTA show a broad distribution of V_{IM} values (see Figure 3.2), however following application of the two dynamic constraints, V_{IM} clusters to the high (less negative) end of the sampling range; a higher V_{IM} is evidently required to support the rate and amount of calcium release required for platelet activation.

The requirement of a resting model configuration approximately remaining at steady state on Ca_{ex} removal necessitates a low resting flux through SOCs. This is coupled with a requirement that following activation SOCE flux rises to levels that are sufficient to elevate $[Ca^{2+}]_{cyt}$ and effects store refilling. These points mean that a model for SOCE needs to have significant cooperativity with respect to decreases in $[Ca^{2+}]_{dts}$. Cooperativity is introduced in three steps. The first is STIM oligomerization following loss of bound DTS Ca^{2+} which is well supported by experiments showing increases in STIM-STIM FRET following store depletion [60, 153]. The second facet of cooperativity comes from graded activation of Orai by association with multiple STIM dimers modeled with Eq. (2.6) [85]. We model STIM-Ca_{dts} association and STIM dimerization with mass action kinetics; this leads to nonzero $STIM_2$ at rest even when stores are full. The third cooperative mechanism, enforcing $STIM_2$ needing to be in the puncta before being able to associate with Orai, is necessary for the model to both have a low enough resting I_{SOC} flux to be stable in EDTA and to simultaneously exhibit appreciable SOCE contribution to $[Ca^{2+}]_{cyt}$ following stimulus (see Figure 3.10). We see a small time delay in peak $[Ca^{2+}]_{cyt}$ compared to simulations run without Ca_{ex} (see Figure 3.3, Figure 3.4 *B* and Figure 3.5) which could conceivably be due to this puncta mechanism because of its dependence on $[Ca^{2+}]_{cyt}$. Fluorescently labeled human platelets stimulated with ADP show $[Ca^{2+}]_{cyt}$ peaking within 5 – 10 s of agonist addition and show little difference in peak time in calcium-containing versus calcium-free conditions (see right panel in Figure 3.5) [150]. However some groups have observed in fluorescently labeled cells following application of thrombin, which is a stronger platelet agonist, a fast rise in $[Ca^{2+}]_{cyt}$ followed by a slower increase [151]. In addition our own group routinely observes a time

difference of about 20 s between agonist delivery and peak $[Ca^{2+}]_{cyt}$ in fluorescently labeled 10% PRP under calcium-free conditions [43].

This lag in SOCE deactivation may be due to missing regulation rather than a deficiency with our method of handling puncta entry. Evidence for alternative regulation of SOCE inactivation has been observed in the literature. Studies have reported that CRACR2A, a transmembrane protein with a cytosol facing EF-hand domain, may be responsible for stabilizing the STIM-Orai complex and that this effect is inhibited at high $[Ca^{2+}]_{cyt}$ [154]. STIM also may be able to interact with phosphoinositides in the PM via its cytosolic polybasic domain. Inhibition of phosphotidylinositol 3-and 4-kinases has been shown to reduce SOCE [155]. However, PIP and PIP_2 levels do not change appreciably in thrombin stimulated platelets [156]. Additionally, many Ca^{2+} channels, including SOCs, are affected by the phenomena of Ca^{2+}-dependent inactivation (CDI) in which Ca^{2+} influx results in local domains of high $[Ca^{2+}]_{cyt}$ which interferes with channel operation [60]. This effect is independent of store refilling [157]. In the future, modeling these regulatory mechanisms may allow for faster SOCE inactivation as stores refill.

Store refilling is often indirectly measured by observing changes in $[Ca^{2+}]_{cyt}$, $[Ca^{2+}]_{dts}$ or I_{SOC} following Ca^{2+} addition in cell populations where stores have been depleted with ionomycin and/or SERCA inhibitors such as thapsigargin [60, 157, 158]; these studies are not reflective of normal store refilling during agonist stimulation. Only a few groups have directly measured $[Ca^{2+}]_{dts}$ versus time in human platelets; this is because most fluorescent calcium dyes are higher affinity dyes designed to measure $[Ca^{2+}]_{cyt}$. One group has used Fluo-5N to measure $[Ca^{2+}]_{dts}$ in human platelets following stimulation with ADP and thrombin, among other compounds [146]. In the absence of

Ca_{ex}, no store refilling was observed following addition of these agonists; our model is consistent with these measurements (see Figure 3.3). This same group observed fast (within 30 s of agonist addition) but partial refilling when thrombin was added to platelets in calcified media. Under strong IP_3 stimulus with Ca_{ex}, our model is capable of 0 to over 100% store refilling depending on the resting configuration. In Figure 3.7 *A* we see the model does not show the amount of fractional refilling of stores being correlated with peak $[Ca^{2+}]_{cyt}$ time. However, Figure 3.7 *B* does show a correlation with the SERCA / IP_3R ratio; taken together with the time courses shown in Figure 3.6, this implies that in order to avoid a significant time delay in $[Ca^{2+}]_{cyt}$, the stores need to refill quickly only to a level such that PMCA can overtake the SOCE flux rather than needing to refill completely. CDI could be modeled to directly cause faster store refilling in early times following activation as high $[Ca^{2+}]_{cyt}$ in puncta microdomains also results in faster SERCA activity in those regions; this scheme would create a scenario of fast store refilling through active SERCA positively regulated by locally higher Ca^{2+} and CDI dependent inactivation followed by a slower inactivation phase (perhaps dependent on residual store refilling through less active SERCA mediated by bulk $[Ca^{2+}]_{cyt}$ and CRACR2A destabilization) which may be important for fully shutting off I_{SOC} in model configurations where stores only partially refill.

Chapter 4

Conclusions and future directions

In this thesis, we have combined kinetic, mechanistic and electrochemical data to produce a computational model of IP_3-mediated calcium release and SOCE in human platelets that can estimate the resting and dynamic behavior of platelets in both calcium-containing and calcium-free conditions. The result is a systems-level model, integrating measurements and observations from dozens of independent studies.

The model presented in this thesis is the first to our knowledge to incorporate a complete mechanism for SOCE into a larger scale systems model of calcium signaling. In Chapter 2 we outlined the model framework, using previous modeling work as a foundation, which casts intracellular Ca^{2+} regulation as a function of the delicate balance between the opposing actions of Ca^{2+} channels and pumps: IP_3R, SERCA, SOCE, and PMCA. The mechanism for SOCE employed mass action kinetics to model Ca^{2+} binding and dimerization of the Ca^{2+} sensor STIM, a $[Ca^{2+}]_{cyt}$ dependent Hill function to determine $STIM_2$ entry into the puncta, and a cooperative equilibrium model to govern the association of $STIM_2$ ligands with the channel-pore forming subunit, Orai.

In Chapter 3 we studied how applying various homeostatic and dynamic constraints affected the preferred resting configuration of the model. The model was able to exhibit physiologic resting states with protein counts and fixed parameters (besides those estimated in this study) close to cited literature values. The model predicted that values of V_{IM}, an experimentally inaccessible quantity, need to be greater than -70 mV in order to achieve calcium release following agonist stimulation (Figure 3.2). The model also possessed a subset of resting configurations that were able to recapitulate experimentally measured $[Ca^{2+}]_{cyt}$ time courses in human platelets under high ADP stimulation (Figure 3.5). The ability of the model to maintain steady state in EDTA was heavily dependent on enforcing physical separation of $STIM_2$ and Orai at rest; increasing the maximum fraction of $STIM_2$ that is able to interact with Orai led to more resting states failing our stability criterion due to raising constitutive leak through SOCs (Figure 3.10). Given the complexity of calcium regulation in biological systems, a cellular signaling model will likely never be fully "complete." In the future, incorporating additional experimental data will allow for more tightly distributed protein copies and will enable the inclusion of downstream platelet functionality such as granule secretion, integrin activation, and phosphatidylserine exposure as well as the modeling of receptors for other important platelet agonists such as thrombin and thromboxane.

There are two logical next steps one could take to further develop the model. The first would be to incorporate calcium dependent inactivation of the STIM-Orai complex as already discussed in Section 3.4. The second direction one could take is motivated by the considerable homology in the activation pathways of the platelet agonists which signal through GPCRs, namely: ADP (via the $P2Y_1$ receptor), thrombin (via the PAR1

and PAR4 receptors) and TxA_2 (via the TP receptor). Following receptor binding, these agonists stimulate Ca^{2+} release from stores via G_q (and G_i to a lesser extent) mediated activation of PLCβ isoforms leading to phosphoinositide hydrolysis and IP_3 generation [5]. Upstream data on ADP mediated IP_3 generation is already available from previous modeling work [57]. Platelets experience these chemical cues simultaneously (among others such as collagen which signals through GPVI and integrin α2β1). Most groups still only measure the response of platelets to one agonist at a time; however, high-throughput "Pairwise Agonist Scanning" techniques have recently been developed to yield high resolution Ca^{2+} fluorescence time course data on PRP stimulated with multiple agonists simultaneously [43]. This technique has produced sufficient data to train neural networks which have been used to model platelet activation in a multiscale lattice kinetic Monte Carlo simulation of platelet aggregation under flow conditions [44] and these works have already demonstrated the synergistic or non-additive effects applying combinations these agonists have on platelets' calcium responses.

One of the themes of the first chapter was how simple behaviors or mechanisms can interact in nonlinear fashions to produce complex outputs or unexpected results. In that vein, unexpected behaviors or interesting new predictions may result from modeling PAR1, PAR4 and TP simply as three receptors of differing copy numbers and ligand affinities, all sharing the same downstream signaling pathways.

Cell signaling networks are studied in a laboratory setting by delivering inputs to cells (e.g. agonists) and then observing some measureable output, such as fluorescence over time in cells labeled with a Ca^{2+} sensitive dye like fura-2. Accurate, mechanistic, systems-level computational models of these networks serve as an invaluable partner to

these wet-lab experiments by allowing one to probe the effects of altering the internal workings of the system (i.e. a cell) on the output in a manner which may be technically infeasible or impossible to do in a laboratory setting. In this way a systems model can serve as a platform from which one can gain a greater understanding of biology and guide future investigations of signaling pathways. With the amount of biological knowledge becoming increasingly vast, computational models will likely take on an even more important role going forward. Even with the advent of high-throughput experimental techniques it is infeasible to explore the entire reaction network in cells (much less model it). In light of this limitation, in the future systems models should serve both as a guide to biologists as to which problems to solve and as a tool in interpreting complex experimental results.

APPENDIX

Appendix A. Analytical solutions to the MWC equations

The system of equations given by Eq. (2.6) in Section 2.4.2 which govern the association of $(STIM_2)_p$ and Orai and set the distribution of SOC channel states do not have a closed form solution in terms of Orai and $(STIM_2)_p$. The ten channel states were solved for analytically in terms of S_f, the amount of STIM in the puncta which is not bound to Orai, using the MATLAB Symbolic Toolbox. These solutions are listed below; $Orai_T$ is the number of Orai tetramers in the system (and was one of the quantities that were allowed to vary during parameter scan sweeps).

$$C = \frac{Orai_T}{Denom}$$
$$CS = 4K_a S_f \left(\frac{Orai_T}{Denom}\right)$$
$$CS_2 = 6aK_a^2 S_f^2 \left(\frac{Orai_T}{Denom}\right)$$
$$CS_3 = 4a^3 K_a^3 S_f^3 \left(\frac{Orai_T}{Denom}\right)$$
$$CS_4 = a^6 K_a^4 S_f^4 \left(\frac{Orai_T}{Denom}\right)$$

$$O = L\left(\frac{Orai_T}{Denom}\right)$$
$$OS = 4LfS_f \left(\frac{Orai_T}{Denom}\right)$$
$$OS_2 = 6aLf^2 S_f^2 \left(\frac{Orai_T}{Denom}\right)$$
$$OS_3 = 4a^3 Lf^3 S_f^3 \left(\frac{Orai_T}{Denom}\right)$$
$$OS_4 = a^6 Lf^4 S_f^4 \left(\frac{Orai_T}{Denom}\right)$$

where '*Denom*' is equal to

$$Denom = 1 + L + 4K_a S_f + 4LfS_f + 6aK_a^2 S_f^2 + 6aLf^2 S_f^2 + 4a^3 K_a^3 S_f^3 + 4a^3 Lf^3 S_f^3 + a^6 K_a^4 S_f^4 + a^6 Lf^4 S_f^4$$

Appendix B. Summary of algebraic IP_3 forcing function parameters

Max fold increase*	a	b	c	t_{max} (s)
1.5	0.03	0.06	0.15	12.7
2	0.1	0.06	0.2	11.2
3	0.3	0.08	0.38	8.3
5	0.7	0.08	0.4	7.9
8	1.35	0.08	0.4	7.8
10	1.75	0.08	0.4	7.2

*Values are approximate.

Table A.1 Exponential forcing function parameter sets.

Lists sets of parameters capable of eliciting various maximal fold increases in $[IP_3]$ using the algebraic forcing function given by Eq. (2.8) in Section 2.5. The time gap between the beginning of the IP_3 stimulus and maximal $[IP_3]$ is indicated in the last column.

BIBLIOGRAPHY

1. Tyson, J.J., *The Belousov-Zhabotinskii reaction*. Lecture notes in biomathematics. 1976, Berlin ; New York: Springer-Verlag. ix, 128 p.

2. Kicheva, A., M. Cohen, and J. Briscoe, *Developmental pattern formation: insights from physics and biology.* Science, 2012. **338**(6104): p. 210-2.

3. Young, D., J. Stark, and D. Kirschner, *Systems biology of persistent infection: tuberculosis as a case study.* Nat Rev Microbiol, 2008. **6**(7): p. 520-8.

4. Go, A.S., et al., *Heart disease and stroke statistics--2013 update: a report from the American Heart Association.* Circulation, 2013. **127**(1): p. e6-e245.

5. Brass, L.F., et al., *Signal transduction during platelet plug formation.*, in *Platelets*. 2007. p. 319-346.

6. Rink, T.J. and S.O. Sage, *Calcium signaling in human platelets.* Annu Rev Physiol, 1990. **52**: p. 431-449.

7. Siess, W., *Molecular mechanisms of platelet activation.* Physiol Rev, 1989. **69**(1): p. 58-178.

8. Brass, L.F. and T.J. Stalker, *Mechanisms of Platelet Activation*, in *Platelets in hematologic and cardiovascular disorders : a clinical handbook*, P. Gresele, Editor. 2008, Cambridge University Press: Cambridge, UK ; New York. p. xiii, 511 p.

9. Crittenden, J.R., et al., *CalDAG-GEFI integrates signaling for platelet aggregation and thrombus formation.* Nat Med, 2004. **10**(9): p. 982-6.

10. Hathaway, D.R. and R.S. Adelstein, *Human platelet myosin light chain kinase requires the calcium-binding protein calmodulin for activity.* Proc Natl Acad Sci U S A, 1979. **76**(4): p. 1653-7.

11. Klages, B., et al., *Activation of G12/G13 results in shape change and Rho/Rho-kinase-mediated myosin light chain phosphorylation in mouse platelets.* J Cell Biol, 1999. **144**(4): p. 745-54.

12. Coppinger, J.A., et al., *Characterization of the proteins released from activated platelets leads to localization of novel platelet proteins in human atherosclerotic lesions.* Blood, 2004. **103**(6): p. 2096-104.

13. Flaumenhaft, R., *Molecular Basis of Platelet Granule Secretion.* Arteriosclerosis, Thrombosis, and Vascular Biology, 2003. **23**(7): p. 1152-1160.

14. Brass, L.F. and S.K. Joseph, *A role for inositol triphosphate in intracellular Ca2+ mobilization and granule secretion in platelets.* J Biol Chem, 1985. **260**(28): p. 15172-9.

15. Schoenwaelder, S.M., et al., *Two distinct pathways regulate platelet phosphatidylserine exposure and procoagulant function.* Blood, 2009. **114**(3): p. 663-6.

16. Braun, A., et al., *Orai1 (CRACM1) is the platelet SOC channel and essential for pathological thrombus formation.* Blood, 2009. **113**(9): p. 2056-63.

17. Tschope, D., P. Rosen, and F.A. Gries, *Increase in the cytosolic concentration of calcium in platelets of diabetics type II.* Thromb Res, 1991. **62**(5): p. 421-8.

18. Vinik, A.I., et al., *Platelet dysfunction in type 2 diabetes.* Diabetes Care, 2001. **24**(8): p. 1476-85.

19. Erne, P., et al., *Correlation of platelet calcium with blood pressure. Effect of antihypertensive therapy.* N Engl J Med, 1984. **310**(17): p. 1084-8.

20. Van Geet, C., et al., *Human platelet pathology related to defects in the G-protein signaling cascade.* J Thromb Haemost, 2009. **7 Suppl 1**: p. 282-6.

21. Rao, A.K. and J. Gabbeta, *Congenital disorders of platelet signal transduction.* Arterioscler Thromb Vasc Biol, 2000. **20**(2): p. 285-9.

22. Michelson, A.D., ed. *Platelets*. 2nd ed. 2007, Academic Press/Elsevier: Amsterdam ; Boston. xlii, 1343 p.

23. Berridge, M.J., M.D. Bootman, and H.L. Roderick, *Calcium signalling: dynamics, homeostasis and remodelling.* Nat Rev Mol Cell Biol, 2003. **4**(7): p. 517-29.

24. Rao, C.V., J.R. Kirby, and A.P. Arkin, *Design and diversity in bacterial chemotaxis: a comparative study in Escherichia coli and Bacillus subtilis.* PLoS Biol, 2004. **2**(2): p. E49.

25. Korobkova, E., et al., *From molecular noise to behavioural variability in a single bacterium.* Nature, 2004. **428**(6982): p. 574-8.

26. Asakura, S. and H. Honda, *Two-state model for bacterial chemoreceptor proteins. The role of multiple methylation.* J Mol Biol, 1984. **176**(3): p. 349-67.

27. Smith, A.E., et al., *Systems analysis of Ran transport.* Science, 2002. **295**(5554): p. 488-91.

28. Gorlich, D., M.J. Seewald, and K. Ribbeck, *Characterization of Ran-driven cargo transport and the RanGTPase system by kinetic measurements and computer simulation.* EMBO J, 2003. **22**(5): p. 1088-100.

29. Riddick, G. and I.G. Macara, *A systems analysis of importin-{alpha}-{beta} mediated nuclear protein import.* J Cell Biol, 2005. **168**(7): p. 1027-38.

30. Hucka, M., et al., *The systems biology markup language (SBML): a medium for representation and exchange of biochemical network models.* Bioinformatics, 2003. **19**(4): p. 524-31.

31. Hartwell, L.H., et al., *From molecular to modular cell biology.* Nature, 1999. **402**(6761 Suppl): p. C47-52.

32. Sorger, P.K., *A reductionist's systems biology: opinion.* Curr Opin Cell Biol, 2005. **17**(1): p. 9-11.

33. Mogilner, A., R. Wollman, and W.F. Marshall, *Quantitative modeling in cell biology: what is it good for?* Dev Cell, 2006. **11**(3): p. 279-87.

34. Gillespie, D.T., *Exact stochastic simulation of coupled chemical reactions.* The Journal of Physical Chemistry, 1977. **81**(25): p. 2340-2361.

35. Linderman, J.J., *Modeling of G-protein-coupled receptor signaling pathways.* J Biol Chem, 2009. **284**(9): p. 5427-31.

36. Bhalla, U.S. and R. Iyengar, *Emergent properties of networks of biological signaling pathways.* Science, 1999. **283**(5400): p. 381-7.

37. Tyson, J.J., A. Csikasz-Nagy, and B. Novak, *The dynamics of cell cycle regulation.* Bioessays, 2002. **24**(12): p. 1095-109.

38. Chen, K.C., et al., *Integrative analysis of cell cycle control in budding yeast.* Mol Biol Cell, 2004. **15**(8): p. 3841-62.

39. De Vries, G. and A. Sherman, *Channel sharing in pancreatic beta -cells revisited: enhancement of emergent bursting by noise.* J Theor Biol, 2000. **207**(4): p. 513-30.

40. Janes, K.A. and M.B. Yaffe, *Data-driven modelling of signal-transduction networks.* Nat Rev Mol Cell Biol, 2006. **7**(11): p. 820-8.

41. Pe'er, D., *Bayesian network analysis of signaling networks: a primer.* Sci STKE, 2005. **2005**(281): p. pl4.

42. Sachs, K., et al., *Causal protein-signaling networks derived from multiparameter single-cell data.* Science, 2005. **308**(5721): p. 523-9.

43. Chatterjee, M.S., et al., *Pairwise agonist scanning predicts cellular signaling responses to combinatorial stimuli.* Nat Biotechnol, 2010. **28**(7): p. 727-32.

44. Flamm, M.H., et al., *Multiscale prediction of patient-specific platelet function under flow.* Blood, 2012. **120**(1): p. 190-8.

45. Moles, C.G., P. Mendes, and J.R. Banga, *Parameter estimation in biochemical pathways: a comparison of global optimization methods.* Genome Res, 2003. **13**(11): p. 2467-74.

46. Vaz, A.I.F. and L.N. Vicente, *A particle swarm pattern search method for bound constrained global optimization.* Journal of Global Optimization, 2007. **39**(2): p. 197-219.

47. Kirkpatrick, S., C.D. Gelatt, Jr., and M.P. Vecchi, *Optimization by simulated annealing.* Science, 1983. **220**(4598): p. 671-80.

48. Kirkilionis, M., *Exploration of cellular reaction systems.* Brief Bioinform, 2010. **11**(1): p. 153-178.

49. Mezer, A., et al., *Systematic search for the rate constants that control the exocytotic process from chromaffin cells by a genetic algorithm.* Biochim Biophys Acta, 2006. **1763**(4): p. 345-55.

50. Degenring, D., et al., *Sensitivity analysis for the reduction of complex metabolism models.* Journal of Process Control, 2004. **14**(7): p. 729-745.

51. Kinzer-Ursem, T.L. and J.J. Linderman, *Both ligand- and cell-specific parameters control ligand agonism in a kinetic model of g protein-coupled receptor signaling.* PLoS Comput Biol, 2007. **3**(1): p. e6.

52. Song, S.O. and J. Varner, *Modeling and analysis of the molecular basis of pain in sensory neurons.* PLoS One, 2009. **4**(9): p. e6758.

53. Vora, N. and P. Daoutidis, *Nonlinear model reduction of chemical reaction systems.* Aiche Journal, 2001. **47**(10): p. 2320-2332.

54. Levitzki, A., *Targeting signal transduction for disease therapy.* Curr Opin Cell Biol, 1996. **8**(2): p. 239-44.

55. Paul, S.M., et al., *How to improve R&D productivity: the pharmaceutical industry's grand challenge.* Nat Rev Drug Discov, 2010. **9**(3): p. 203-14.

56. Lenoci, L., et al., *Mathematical model of PAR1-mediated activation of human platelets.* Mol Biosyst, 2011. **7**(4): p. 1129-37.

57. Purvis, J.E., et al., *A molecular signaling model of platelet phosphoinositide and calcium regulation during homeostasis and P2Y1 activation.* Blood, 2008. **112**(10): p. 4069-4079.

58. Purvis, J.E., R. Radhakrishnan, and S.L. Diamond, *Steady-state kinetic modeling constrains cellular resting states and dynamic behavior.* PLoS Comput Biol, 2009. **5**(3): p. e1000298.

59. Juska, A., *Plasma membrane calcium pump and sodium-calcium exchanger in maintenance and control of calcium concentrations in platelets.* Biochem Biophys Res Commun, 2010. **392**(1): p. 41-6.

60. Lewis, R.S., *Store-operated calcium channels: new perspectives on mechanism and function.* Cold Spring Harb Perspect Biol, 2011. **3**(12).

61. Putney, J.W., Jr., *A model for receptor-regulated calcium entry.* Cell Calcium, 1986. **7**(1): p. 1-12.

62. Hoth, M. and R. Penner, *Depletion of intracellular calcium stores activates a calcium current in mast cells.* Nature, 1992. **355**(6358): p. 353-6.

63. Prakriya, M., *Regulation of CRAC Channel Activity by Recruitment of Silent Channels to a High Open-probability Gating Mode.* The Journal of General Physiology, 2006. **128**(3): p. 373-386.

64. Zweifach, A. and R.S. Lewis, *Mitogen-regulated Ca2+ current of T lymphocytes is activated by depletion of intracellular Ca2+ stores.* Proc Natl Acad Sci U S A, 1993. **90**(13): p. 6295-9.

65. Liou, J., et al., *STIM is a Ca2+ sensor essential for Ca2+-store-depletion-triggered Ca2+ influx.* Curr Biol, 2005. **15**(13): p. 1235-41.

66. Mercer, J.C., et al., *Large store-operated calcium selective currents due to co-expression of Orai1 or Orai2 with the intracellular calcium sensor, Stim1.* J Biol Chem, 2006. **281**(34): p. 24979-90.

67. Wu, M.M., et al., *Ca2+ store depletion causes STIM1 to accumulate in ER regions closely associated with the plasma membrane.* J Cell Biol, 2006. **174**(6): p. 803-13.

68. Baba, Y., et al., *Coupling of STIM1 to store-operated Ca2+ entry through its constitutive and inducible movement in the endoplasmic reticulum.* Proc Natl Acad Sci U S A, 2006. **103**(45): p. 16704-9.

69. Liou, J., et al., *Live-cell imaging reveals sequential oligomerization and local plasma membrane targeting of stromal interaction molecule 1 after Ca2+ store depletion.* Proc Natl Acad Sci U S A, 2007. **104**(22): p. 9301-6.

70. Zhang, S.L., et al., *STIM1 is a Ca2+ sensor that activates CRAC channels and migrates from the Ca2+ store to the plasma membrane.* Nature, 2005. **437**(7060): p. 902-5.

71. Stathopulos, P.B., et al., *Stored Ca2+ depletion-induced oligomerization of stromal interaction molecule 1 (STIM1) via the EF-SAM region: An initiation mechanism for capacitive Ca2+ entry.* J Biol Chem, 2006. **281**(47): p. 35855-62.

72. Homer, R. Fagles, and B. Knox, *The Iliad*. 1990, New York, N.Y., U.S.A.: Viking. xvi, 683 p.

73. Feske, S., et al., *A mutation in Orai1 causes immune deficiency by abrogating CRAC channel function.* Nature, 2006. **441**(7090): p. 179-85.

74. Vig, M., et al., *CRACM1 is a plasma membrane protein essential for store-operated Ca2+ entry.* Science, 2006. **312**(5777): p. 1220-3.

75. Zhang, S.L., et al., *Genome-wide RNAi screen of Ca(2+) influx identifies genes that regulate Ca(2+) release-activated Ca(2+) channel activity.* Proc Natl Acad Sci U S A, 2006. **103**(24): p. 9357-62.

76. Putney, J.W., *The Physiological Function of Store-operated Calcium Entry.* Neurochem Res, 2011.

77. Varga-Szabo, D., et al., *The calcium sensor STIM1 is an essential mediator of arterial thrombosis and ischemic brain infarction.* Journal of Experimental Medicine, 2008. **205**(7): p. 1583-1591.

78. Luik, R.M., et al., *The elementary unit of store-operated Ca2+ entry: local activation of CRAC channels by STIM1 at ER-plasma membrane junctions.* J Cell Biol, 2006. **174**(6): p. 815-25.

79. Derler, I., et al., *Increased hydrophobicity at the N terminus/membrane interface impairs gating of the severe combined immunodeficiency-related ORAI1 mutant.* J Biol Chem, 2009. **284**(23): p. 15903-15.

80. Fahrner, M., et al., *Mechanistic view on domains mediating STIM1-Orai coupling.* Immunol Rev, 2009. **231**(1): p. 99-112.

81. Muik, M., et al., *Dynamic coupling of the putative coiled-coil domain of ORAI1 with STIM1 mediates ORAI1 channel activation.* J Biol Chem, 2008. **283**(12): p. 8014-22.

82. Yuan, J.P., et al., *SOAR and the polybasic STIM1 domains gate and regulate Orai channels.* Nat Cell Biol, 2009. **11**(3): p. 337-43.

83. Park, C.Y., et al., *STIM1 Clusters and Activates CRAC Channels via Direct Binding of a Cytosolic Domain to Orai1*. Cell, 2009. **136**(5): p. 876-890.

84. Li, Z., et al., *Graded activation of CRAC channel by binding of different numbers of STIM1 to Orai1 subunits.* Cell Res, 2011. **21**(2): p. 305-15.

85. Hoover, P.J. and R.S. Lewis, *Stoichiometric requirements for trapping and gating of Ca2+ release-activated Ca2+ (CRAC) channels by stromal interaction molecule 1 (STIM1).* Proc Natl Acad Sci U S A, 2011.

86. Soboloff, J., et al., *Orai1 and STIM reconstitute store-operated calcium channel function.* J Biol Chem, 2006. **281**(30): p. 20661-5.

87. Peinelt, C., et al., *Amplification of CRAC current by STIM1 and CRACM1 (Orai1).* Nature Cell Biology, 2006. **8**(7): p. 771-773.

88. Li, Z., et al., *Mapping the interacting domains of STIM1 and Orai1 in Ca2+ release-activated Ca2+ channel activation.* J Biol Chem, 2007. **282**(40): p. 29448-56.

89. Yang, S., J.J. Zhang, and X.Y. Huang, *Orai1 and STIM1 are critical for breast tumor cell migration and metastasis.* Cancer Cell, 2009. **15**(2): p. 124-34.

90. Abdullaev, I.F., et al., *Stim1 and Orai1 mediate CRAC currents and store-operated calcium entry important for endothelial cell proliferation.* Circ Res, 2008. **103**(11): p. 1289-99.

91. Stiber, J., et al., *STIM1 signalling controls store-operated calcium entry required for development and contractile function in skeletal muscle.* Nat Cell Biol, 2008. **10**(6): p. 688-97.

92. Berra-Romani, R., et al., *Ca2+ handling is altered when arterial myocytes progress from a contractile to a proliferative phenotype in culture.* Am J Physiol Cell Physiol, 2008. **295**(3): p. C779-90.

93. Potier, M., et al., *Evidence for STIM1- and Orai1-dependent store-operated calcium influx through ICRAC in vascular smooth muscle cells: role in proliferation and migration.* FASEB J, 2009. **23**(8): p. 2425-37.

94. Bergmeier, W., et al., *R93W mutation in Orai1 causes impaired calcium influx in platelets.* Blood, 2009. **113**(3): p. 675-8.

95. Schoenwaelder, S.M., Y. Yuan, and S.P. Jackson, *Calpain regulation of integrin alpha IIb beta 3 signaling in human platelets.* Platelets, 2000. **11**(4): p. 189-98.

96. Vandenberghe, M., et al., *ORAI1 calcium channel orchestrates skin homeostasis.* Proc Natl Acad Sci U S A, 2013.

97. Varga-Szabo, D., A. Braun, and B. Nieswandt, *Calcium signaling in platelets.* J Thromb Haemost, 2009. **7**(7): p. 1057-66.

98. Dolan, A.T. and S.L. Diamond, *Systems modeling of calcium homeostasis and mobilization in platelets mediated by IP3 and store-operated calcium entry.* Biophysical Journal, 2014. **106**(9): p. 1-12. In Press.

99. Burkhart, J.M., et al., *The first comprehensive and quantitative analysis of human platelet protein composition allows the comparative analysis of structural and functional pathways.* Blood, 2012. **120**(15): p. e73-82.

100. Kholodenko, B.N., et al., *Quantification of short term signaling by the epidermal growth factor receptor.* J Biol Chem, 1999. **274**(42): p. 30169-81.

101. Heemskerk, J.W., et al., *Ragged spiking of free calcium in ADP-stimulated human platelets: regulation of puff-like calcium signals in vitro and ex vivo.* J Physiol, 2001. **535**(Pt 3): p. 625-35.

102. Schmidt, H. and M. Jirstrand, *Systems Biology Toolbox for MATLAB: a computational platform for research in systems biology.* Bioinformatics, 2006. **22**(4): p. 514-5.

103. Dode, L., et al., *Dissection of the functional differences between sarco(endo)plasmic reticulum Ca2+-ATPase (SERCA) 1 and 3 isoforms by steady-state and transient kinetic analyses.* J Biol Chem, 2002. **277**(47): p. 45579-91.

104. Sneyd, J. and J.F. Dufour, *A dynamic model of the type-2 inositol trisphosphate receptor.* Proc Natl Acad Sci U S A, 2002. **99**(4): p. 2398-403.

105. Dean, W.L., et al., *Regulation of platelet plasma membrane Ca2+-ATPase by cAMP-dependent and tyrosine phosphorylation.* J Biol Chem, 1997. **272**(24): p. 15113-9.

106. Caride, A.J., et al., *The Plasma Membrane Ca2+ Pump Isoform 4a Differs from Isoform 4b in the Mechanism of Calmodulin Binding and Activation Kinetics: IMPLICATIONS FOR Ca2+ SIGNALING.* Journal of Biological Chemistry, 2007. **282**(35): p. 25640-25648.

107. Brini, M. and E. Carafoli, *The plasma membrane Ca(2)+ ATPase and the plasma membrane sodium calcium exchanger cooperate in the regulation of cell calcium.* Cold Spring Harb Perspect Biol, 2011. **3**(2).

108. White, J.G., *Platelet Structure*, in *Platelets*. 2007. p. 45-73.

109. Ebbeling, L., et al., *Rapid ultrastructural changes in the dense tubular system following platelet activation.* Blood, 1992. **80**(3): p. 718-23.

110. Alberts, B., *Molecular biology of the cell*. 4th ed. 2002, New York: Garland Science. xxxiv, 1548 p.

111. Hodgkin, A.L. and A.F. Huxley, *A quantitative description of membrane current and its application to conduction and excitation in nerve. 1952.* Bull Math Biol, 1990. **52**(1-2): p. 25-71; discussion 5-23.

112. Adelman, W.J., *Biophysics and physiology of excitable membranes*. 1971, New York,: Van Nostrand Reinhold Co. xiv, 527 p.

113. Mahaut-Smith, M.P., et al., *Properties of the demarcation membrane system in living rat megakaryocytes.* Biophys J, 2003. **84**(4): p. 2646-54.

114. Mahaut-Smith, M.P., et al., *Voltage-gated potassium channels and the control of membrane potential in human platelets.* J Physiol, 1990. **428**: p. 723-735.

115. MacIntyre, D.E. and T.J. Rink, *The role of platelet membrane potential in the initiation of platelet aggregation.* Thromb Haemost, 1982. **47**(1): p. 22-26.

116. Burdakov, D., O. Petersen, and A. Verkhratsky, *Intraluminal calcium as a primary regulator of endoplasmic reticulum function.* Cell Calcium, 2005. **38**(3-4): p. 303-310.

117. Mogami, H., A.V. Tepikin, and O.H. Petersen, *Termination of cytosolic Ca2+ signals: Ca2+ reuptake into intracellular stores is regulated by the free Ca2+ concentration in the store lumen.* EMBO J, 1998. **17**(2): p. 435-42.

118. Solovyova, N., et al., *Ca(2+) dynamics in the lumen of the endoplasmic reticulum in sensory neurons: direct visualization of Ca(2+)-induced Ca(2+) release triggered by physiological Ca(2+) entry.* EMBO J, 2002. **21**(4): p. 622-30.

119. Roos, J., et al., *STIM1, an essential and conserved component of store-operated Ca2+ channel function.* J Cell Biol, 2005. **169**(3): p. 435-45.

120. Thompson, J.L. and T.J. Shuttleworth, *How many Orai's does it take to make a CRAC channel?* Scientific reports, 2013. **3**: p. 1961.

121. Mignen, O., J.L. Thompson, and T.J. Shuttleworth, *Orai1 subunit stoichiometry of the mammalian CRAC channel pore.* J Physiol, 2008. **586**(2): p. 419-25.

122. Luik, R.M., et al., *Oligomerization of STIM1 couples ER calcium depletion to CRAC channel activation.* Nature, 2008. **454**(7203): p. 538-542.

123. Varga-Szabo, D., A. Braun, and B. Nieswandt, *STIM and Orai in platelet function.* Cell Calcium, 2011. **50**(3): p. 270-8.

124. Calloway, N., et al., *Molecular clustering of STIM1 with Orai1/CRACM1 at the plasma membrane depends dynamically on depletion of Ca2+ stores and on electrostatic interactions.* Mol Biol Cell, 2009. **20**(1): p. 389-99.

125. Barr, V.A., et al., *Formation of STIM and Orai complexes: puncta and distal caps.* Immunol Rev, 2009. **231**(1): p. 148-59.

126. Rosado, J.A., S. Jenner, and S.O. Sage, *A role for the actin cytoskeleton in the initiation and maintenance of store-mediated calcium entry in human platelets. Evidence for conformational coupling.* J Biol Chem, 2000. **275**(11): p. 7527-33.

127. Monod, J., J. Wyman, and J.P. Changeux, *On the Nature of Allosteric Transitions: A Plausible Model.* J Mol Biol, 1965. **12**: p. 88-118.

128. Hokin, L.E., *Receptors and phosphoinositide-generated second messengers.* Annual review of biochemistry, 1985. **54**: p. 205-35.

129. Putney, J.W., Jr., et al., *Formation and biological action of inositol 1,4,5-trisphosphate.* Federation proceedings, 1986. **45**(11): p. 2634-8.

130. Daniel, J.L., et al., *Molecular basis for ADP-induced platelet activation. I. Evidence for three distinct ADP receptors on human platelets.* J Biol Chem, 1998. **273**(4): p. 2024-9.

131. Kahaner, D., et al., *Numerical methods and software*. 1988, Englewood Cliffs, N.J.: Prentice Hall. xii, 495 p.

132. Yang, X., et al., *Human platelet signaling defect characterized by impaired production of inositol-1,4,5-triphosphate and phosphatidic acid and diminished Pleckstrin phosphorylation: evidence for defective phospholipase C activation.* Blood, 1996. **88**(5): p. 1676-83.

133. Andrews, S.S. and A.P. Arkin, *Simulating cell biology.* Curr Biol, 2006. **16**(14): p. R523-7.

134. Asthagiri, A.R. and D.A. Lauffenburger, *Bioengineering models of cell signaling.* Annu Rev Biomed Eng, 2000. **2**: p. 31-53.

135. Discala, C., et al., *DBcat: a catalog of 500 biological databases.* Nucleic Acids Res, 2000. **28**(1): p. 8-9.

136. Matthews, L., et al., *Reactome knowledgebase of human biological pathways and processes.* Nucleic Acids Res, 2009. **37**(Database issue): p. D619-22.

137. Sivakumaran, S., et al., *The Database of Quantitative Cellular Signaling: management and analysis of chemical kinetic models of signaling networks.* Bioinformatics, 2003. **19**(3): p. 408-15.

138. Dode, L., et al., *Dissection of the functional differences between sarco(endo)plasmic reticulum Ca2+-ATPase (SERCA) 1 and 2 isoforms and characterization of Darier disease (SERCA2) mutants by steady-state and transient kinetic analyses.* J Biol Chem, 2003. **278**(48): p. 47877-89.

139. Ingram, P.J., M.P. Stumpf, and J. Stark, *Network motifs: structure does not determine function.* BMC Genomics, 2006. **7**: p. 108.

140. Press, W.H., *Numerical recipes in C++ : the art of scientific computing*. 2nd ed. 2002, Cambridge, UK ; New York: Cambridge University Press. xxvii, 1002 p.

141. Brewer, D., et al., *Fitting ordinary differential equations to short time course data.* Philos Transact A Math Phys Eng Sci, 2008. **366**(1865): p. 519-44.

142. Klamt, S. and J. Stelling, *Stoichiometric and constraint-based modeling*, in *System modeling in cell biology : from concepts to nuts and bolts*, Z. Szallasi, J. Stelling, and V. Periwal, Editors. 2006, MIT Press: Cambridge, Mass. p. xiv, 448 p.

143. Machlus, K.R. and J.E. Italiano, Jr., *The incredible journey: From megakaryocyte development to platelet formation.* J Cell Biol, 2013. **201**(6): p. 785-96.

144. Tarver, A.P., W.G. King, and S.E. Rittenhouse, *Inositol 1,4,5-trisphosphate and inositol 1,2-cyclic 4,5-trisphosphate are minor components of total mass of inositol trisphosphate in thrombin-stimulated platelets. Rapid formation of inositol 1,3,4-trisphosphate.* J Biol Chem, 1987. **262**(36): p. 17268-71.

145. Nakagawa, T., et al., *Ketamine suppresses platelet aggregation possibly by suppressed inositol triphosphate formation and subsequent suppression of cytosolic calcium increase.* Anesthesiology, 2002. **96**(5): p. 1147-52.

146. Sage, S.O., et al., *Monitoring the intracellular store Ca(2+) concentration in agonist-stimulated, intact human platelets by using Fluo-5N.* J Thromb Haemost, 2011. **9**(3): p. 540-51.

147. Bushinsky, D.A. and R.D. Monk, *Electrolyte quintet: Calcium.* Lancet, 1998. **352**(9124): p. 306-11.

148. Shannon, T.R., K.S. Ginsburg, and D.M. Bers, *Reverse mode of the sarcoplasmic reticulum calcium pump and load-dependent cytosolic calcium decline in voltage-clamped cardiac ventricular myocytes.* Biophys J, 2000. **78**(1): p. 322-33.

149. Bird, G.S., et al., *Methods for studying store-operated calcium entry.* Methods, 2008. **46**(3): p. 204-12.

150. MacKenzie, A.B., M.P. Mahaut-Smith, and S.O. Sage, *Activation of receptor-operated cation channels via P2X1 not P2T purinoceptors in human platelets.* J Biol Chem, 1996. **271**(6): p. 2879-81.

151. Harper, M.T. and A.W. Poole, *Store-operated calcium entry and non-capacitative calcium entry have distinct roles in thrombin-induced calcium signalling in human platelets.* Cell Calcium, 2011.

152. Mark, B.L., et al., *Crystal structure of human beta-hexosaminidase B: understanding the molecular basis of Sandhoff and Tay-Sachs disease.* J Mol Biol, 2003. **327**(5): p. 1093-109.

153. Zhou, Y., et al., *Initial activation of STIM1, the regulator of store-operated calcium entry.* Nat Struct Mol Biol, 2013. **20**(8): p. 973-81.

154. Srikanth, S., et al., *A novel EF-hand protein, CRACR2A, is a cytosolic Ca2+ sensor that stabilizes CRAC channels in T cells.* Nature Cell Biology, 2010. **12**(5): p. 436-446.

155. Rosado, J.A. and S.O. Sage, *Regulation of plasma membrane Ca2+-ATPase by small GTPases and phosphoinositides in human platelets.* J Biol Chem, 2000. **275**(26): p. 19529-35.

156. Wilson, D.B., E.J. Neufeld, and P.W. Majerus, *Phosphoinositide interconversion in thrombin-stimulated human platelets.* J Biol Chem, 1985. **260**(2): p. 1046-51.

157. Parekh, A.B. and J.W. Putney, Jr., *Store-operated calcium channels.* Physiol Rev, 2005. **85**(2): p. 757-810.

158. Brini, M., et al., *Effects of PMCA and SERCA pump overexpression on the kinetics of cell Ca(2+) signalling.* EMBO J, 2000. **19**(18): p. 4926-35.